PRODUCTION OF HOLLOW FIBERS BY CO-ELECTROSPINNING OF CELLULOSE ACETATE

by

Abdurizzagh Khalf

Thesis submitted in partial fulfilment
of the requirements for the degree

of

MASTER OF SCIENCE IN ENGINEERING
(CHEMICAL ENGINEERING)

In the Department of Process Engineering
at the University of Stellenbosch

Study Leaders

Prof JH Knoetze

Prof RD Sanderson

March 2009

Chapter 5

Factorial design experiments

5.1 Introduction

Factorial design allows for the analysis of the effects of several variables, and their integration into a response model [77].

A full 2^4 factorial design was used to determine which factor has the largest effect on the response (ID and OD of the electrospun hollow fibers), and whether there exists any interactions between factors. In a 2^4 design, all combinations of four factors are set at two levels: the two levels are the allowable limits (maximum and minimum values). The inner and outer diameter (ID and OD) of the electrospun hollow fibers were considered as the responses for the different combinations of factor levels. Table 5.1 tabulates the experimental sheet in standard order along with inner and outer diameters of the electrospun hollow fibers. Design Expert v.7 statistical software (Stat Eae Inc.) was used for the analysis of the experimental data.

5.2 Parameters selected

A series of experimental investigations was carried out in order to determine the more important factors that influence the formation of CA hollow fibers. Details of these experiments were reported earlier in Chapter 4 (Section 4.3 and 4.5). The investigations included the consideration of the behaviour of the coaxial jet, the stability of the electrospinning process, and the morphology and structure of the electrospun fibers.

The factors that were found to be most important were: polymer solution concentration (Conc.), shell feed rate (Shell. F), core feed rate (Core.F) and spinning distance (Spinning. D).

Table 5-1: Experiment sheet according to standard order with data

	Factor 1	Factor 2	Factor 3	Factor 4	Response 1	Response 2
Run	A:CA Concentration	B: Core feed rate	C: Shell feed rate	D: Spinning distance	ID	OD
	(wt %)	(ml/hr)	(ml/hr)	(cm)	(nm)	(nm)
1	12	0.5	3	8	352	745
2	14	0.5	1	11	614	1683
3	12	1	3	11	564	1407
4	12	0.5	3	11	540	1622
5	12	1	3	8	507	1736
6	14	1	3	11	1166	3050
7	14	0.5	3	11	1158	2882
8	14	1	1	8	219	970
9	14	0.5	1	11	508	1354
10	14	0.5	3	8	495	1266
11	12	1	1	8	0	——
12	14	1	1	11	0	——
13	14	0.5	1	8	0	——
14	12	1	1	11	0	——
15	12	1	1	8	190	497
16	12	0.5	1	11	0	——
17	12	0.5	1	11	0	——
18	12	0.5	3	8	400	1288.
19	14	1	3	8	960	2291
20	14	1	1	11	398	852.
21	12	1	3	8	497	1713
22	14	0.5	3	11	1016	2340
23	14	1	3	8	1028	2285
24	12	0.5	1	8	0	——
25	12	1	3	11	417	1301
26	12	0.5	1	8	0	——
27	14	0.5	3	8	872	2458
28	14	1	1	8	371	1115
29	12	1	1	11	182	638
30	12	0.5	3	11	417	1132
31	14	0.5	1	8	0	——
32	14	1	3	11	849	2456

In order to increase the confidence of the experiment two replications were used, making 32 runs. This greatly improved the model accuracy.

The SEM images obtained for samples from all 32 runs are shown in Appendix D. Detailed fiber diameter measurements and image analysis procedure were reported earlier in Chapter 3 (Section 3.6.4).

The analysis of the images showed:

1. Most of the fibers electrospun from a high polymer concentration (14 wt %) had higher ID and OD. This indicates that the inner and outer diameters increase with increasing polymer concentration.

2. Most of the fibers electrospun from a low shell feed rate (1 ml/hr) had no core-shell structure, which affected the morphology, quality and diameter of the electrospun fibers. The reason could be that the feed rate of the shell solution was too low to wrap the core solution.

3. Fibers electrospun from a low core feed rate (0.5 ml/hr), high shell feed rate (3 ml/hr) and a low spinning distance (8 cm) are likely to be uniform and have optimum hollow structure.

5.3 Half-normal probability plot

This plot can be used to choose significant effects. In this plot the large absolute values show up as outliers in the upper right-hand section of the plot. The effects can be simply selected by clicking on the square points, starting with the largest effect at the right side of the plot, and selected from right to left until the curve matches up with the majority of the effects near zero.

“Model” is the term that is used in estimating the factor effects (those that fall off the normal probability line of the effects plot (see Appendix C Figure C1).
Figures 5.1 and 5.2 display half-normal probability plots of the effects determined from the model. In Figure 5.1 the effects of A, D, C, AC, AD, BD and ABD are significant effects for ID response, and therefore will be considered for further analysis. Figure 5.2 shows that factors A, B, C, D, AD, BD, ABD and ABCD are the most significant effects for OD response, and therefore will also be considered for further analysis. In both figures an effect is said to be a positive when an increase in its level results in an increase in the response and negative when an increase in its level results in a decrease in the response. The green triangles display the error determined from the replicate.

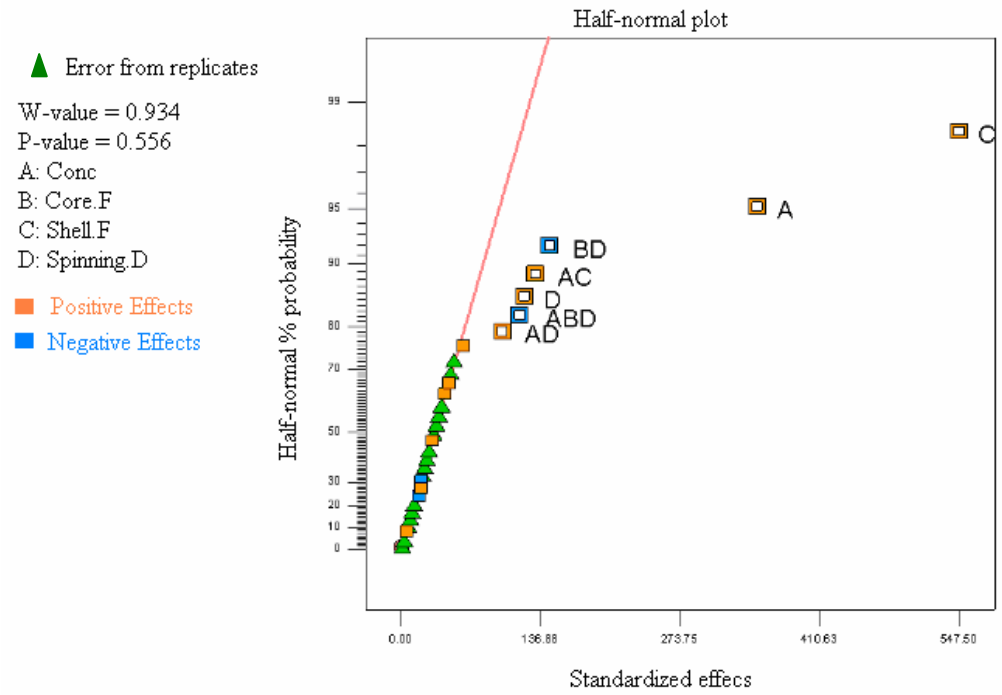

Figure 5.1: Half-normal probability plot of factor effects on ID response.

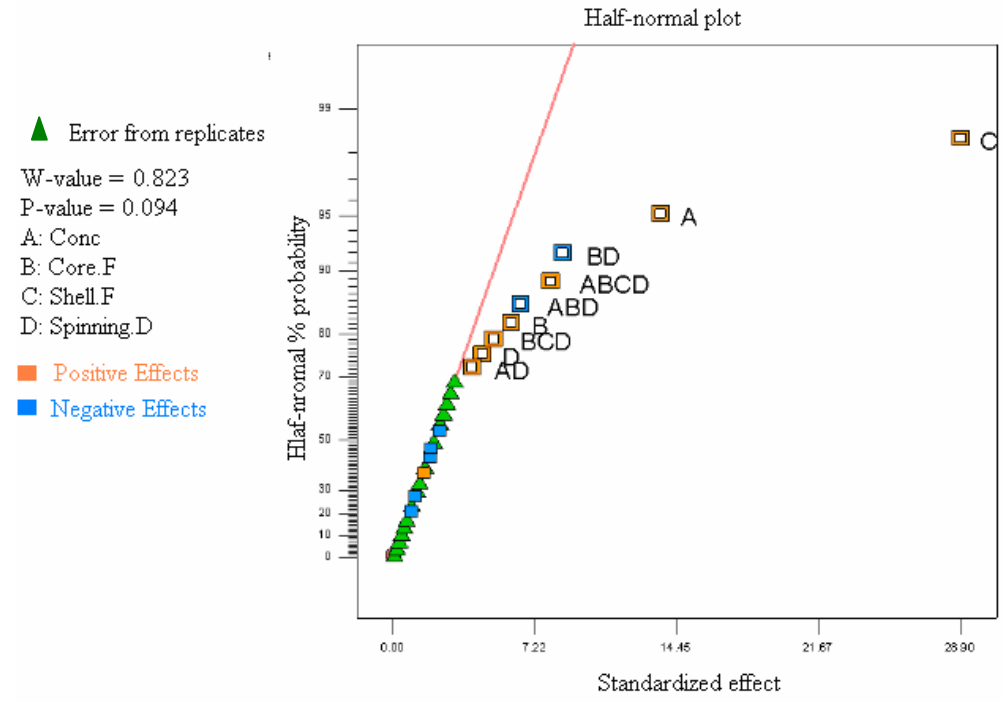

Figure 5.2: Half-normal probability plot of factor effects on OD response.

5.4 Pareto chart

A Pareto chart is used to show the relative size of effects using the t-value scale and conferring a limit to provide a more accurate measure of the relative effects. Effects above the Bonferroni limit [77] are almost certainly significant while the effects above the t-value limit are possibly significant. Effects below the t-value limit are not likely to be significant. The two different t limits are plotted on the chart– based on the Bonferroni corrected t and a standard t. These limits are re-calculated, and change as terms are added or removed from the model. These t-limits are only approximations to the 5 risk level.

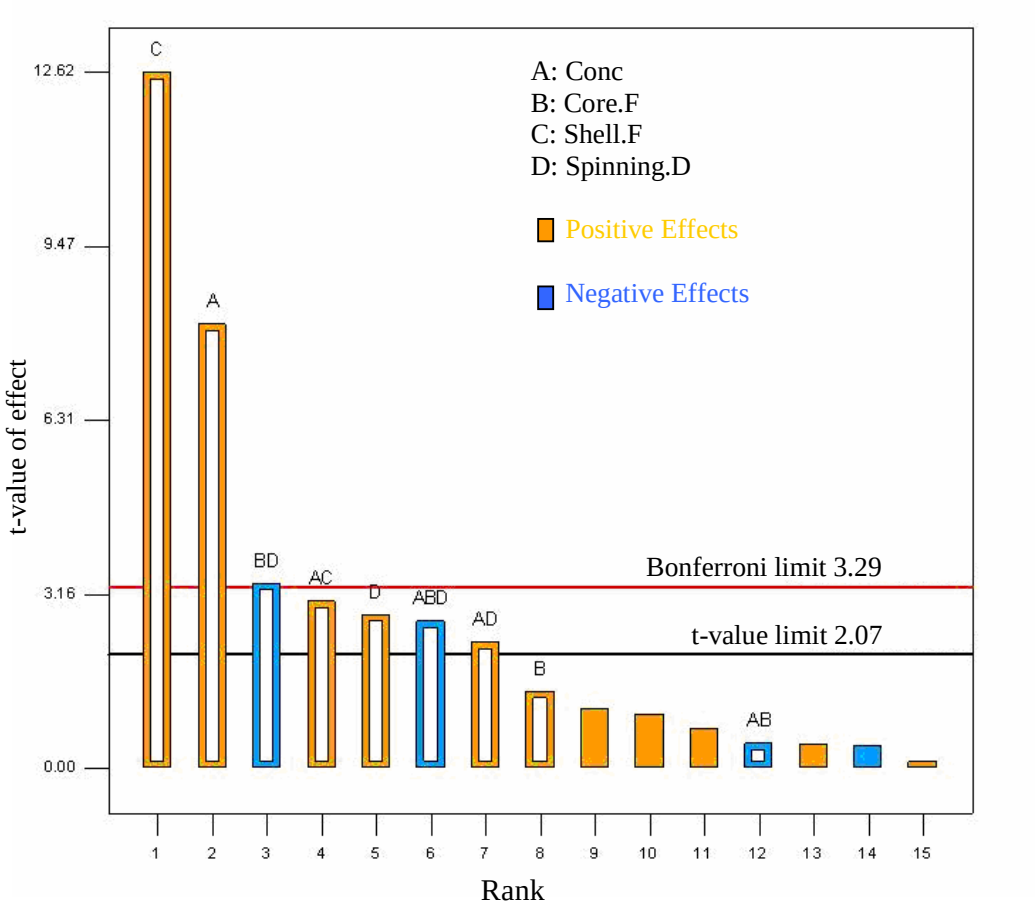

Figure 5.3: Pareto chart of effects (ID analysis).

Figures 5.3 and 5.4 display Pareto chart of effects determined from the model. In Figure 5.3 the effects of A, D, C, AC, AD, BD and ABD are above the t-value limit, and therefore they are significant effects for the ID response, and will be considered for further analysis. Figure 5.4 shows that factors A, B, C, D, AD, BD, ABD and ABCD are above the t-value limit, and therefore they are the most significant effects for the OD response, and will be considered for further analysis. In both figures, an effect is said to be a positive when an increase in its level results in an increase in the response and negative when an increase in its level results in a decrease in the response.

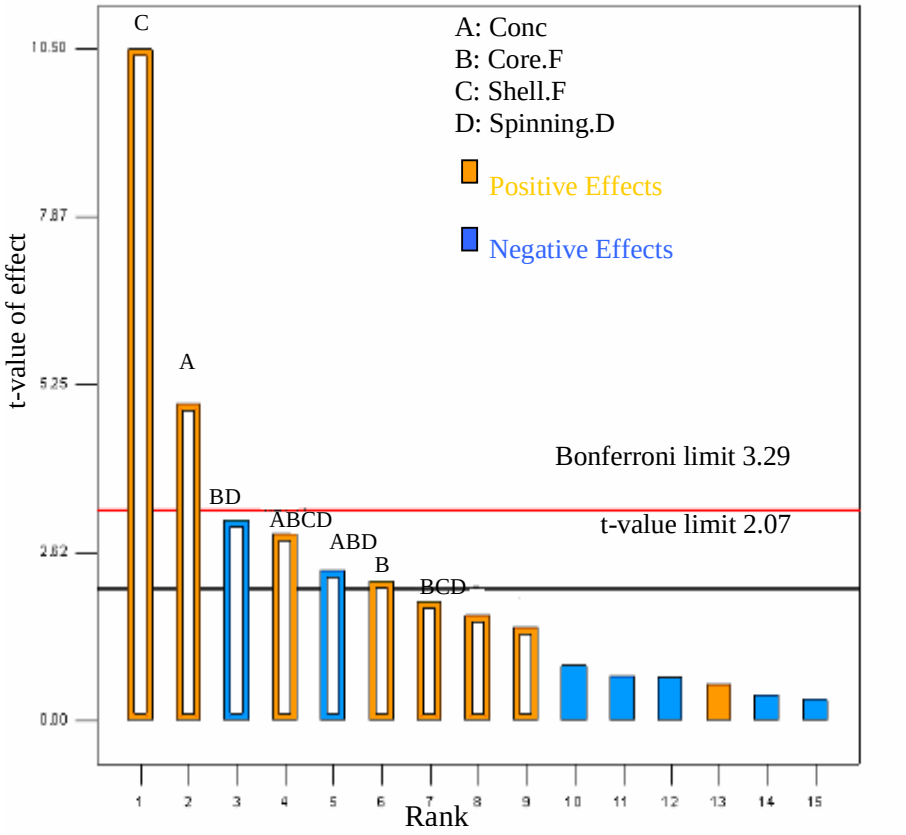

Figure 5.4: Pareto chart of effects (OD analysis).

5.5 Effects

The impact of a factor is indicated by the change in the response as a result of variation in the level of the factor. In a 2^4 factorial design there are four main effects (A, B, C and D) that result from varying a single factor and there are 10 interaction

effects (AB, AC, AD, BC, CD, ABC, ABD, CD, BCD and ABCD) that result from varying two or more factors. The interaction effects take place when the effect of one factor depends on the level of another factor.

Any factors selected from either the half-normal plot or the normal plot will be shown as selected on the effects list. The effects list also reports the sum of the squares and the percentage contribution by each term. The percentage contribution is obtained by adding the total sum of squares and then taking each term's sum of squares and dividing it by the total, to get a percentage [78].

The effects together with their contributions toward the two responses ID and OD are shown in Tables 5-2 and 5-3.

Table 5-2: List of effects and their contributions toward ID

	Term	Effect	SumSqr	% contribution
Model	A-Conc	349.4	976798	22.4
Model	B-Core.F	61	29800.1	0.6
Model	C-Shell.F	547.5	2.39805E+006	55
Model	D-Spinning.D	121.2	117651	2.7
Error	AB	-20	3203	0
Model	AC	131.8	139008	3.1
Model	AD	99.5	79278.8	1.8
Model	BC	31.2	7800.9	0.1
Error	BD	-145.6	169798	3.9
Model	CD	5.8	271.9	0
Model	ABC	43.3	15021.1	0.3
Error	ABD	-116.1	107899	2.4
Error	ACD	-17.9	2579.8	0
Model	BCD	19.8	3143.8	0
Model	ABCD	47.3	17905.6	0.4
Error	Lack of fit		0	0
Error	Pure error		284526	6.5

Table 5-3: List of effects and their contributions toward OD

	Term	Effect	SumSqr	% contribution
Model	A-Conc	13.6	1484.1	12.6
Model	B-Core.F	6	289.4	2.4
Model	C-Shell.F	28.8	6679.9	56.8
Model	D-Spinning.D	4.5	165.2	1.4
Error	AB	-2.3	45	0.3
Error	AC	-1.8	28.2	0.2
Model	AD	4	129	1
Error	BC	-1.9	29.4	0.2
Error	BD	-8.6	596.9	5
Error	CD	-1.1	10.3	0
Model	ABC	1.5	20	0.1
Error	ABD	-6.4	336	2.8
Error	ACD	-0.9	6.8	0
Model	BCD	5.1	211.3	1.7
Model	ABCD	8	516.3	4.3
Error	Lack of fit		0	0
Error	Pure error		1193.3	10.1

"Error" is the term that reveals the effect that was found to be insignificant.
Lack of fit is the term that reveals the variation of the data around the fitted model. Insignificant lack of fit indicates that the model fits well with the data.
Pure error is the term that reveals the normal variation in the response resulting from repeated experiments.

The program (Design Expert) displays a list of all the effects as estimated from the model. Factors with a high level of influence on the response will each show as a high rate of contribution.
The effects as tabulated in Table 5-2 have shown that the shell feed rate is the most important parameter and contributes most significantly to the ID response. The other major contributing factors are the concentration of the shell solution, spinning distance and core feed rate. Similar results were obtained for the OD response, but at different combinations of the factor levels. Interestly, the core feed rate contributed significantly more to the OD than the ID response. It was also found that three and four-interaction effects were involved in this model. These interaction effects are the interaction between shell concentration, core feed rate and spinning distance (ABD) and the interaction between shell concentration, core feed rate, shell feed rate and spinning distance (ABCD), as shown in Table 5-3.

5.6 ANOVA (analysis of variance)

ANOVA is a statistical method that subdivides the whole variation of the set data into unit parts linked with specific sources of variation, for the purpose of testing a hypothesis of a variable on the model [78]. In this model the F-value (the mean square for the term divided by the mean square for the residual) for both responses ID and OD indicated that the model is significant (Tables 5.4 and 5.7). Factor effects with a significant level of 0.05 or lower were included in the model. The ANOVA report for the ID response indicated that shell concentration (A), shell feed rate (C), spinning distance (D), the interaction between shell concentration and shell feed rate (AC), the interaction between shell concentration and spinning distance (AD), the interaction between core feed rate and spinning distance (BD) and the interaction between shell concentration, core feed rate and spinning distance (ABD) are significant model terms (Table 5.4), and for the OD response it showed that shell concentration (A), shell feed rate (C), the interaction between core feed rate and spinning distance (BD), the interaction between shell concentration, core feed rate and spinning distance (ABD) and the interaction between shell concentration, core feed rate, shell feed rate and spinning distance (ABCD) are the significant model terms (Table 5.7).

The significant model term indicates that an increase in effect level results in an increase in the response, while the insignificant model reveals that an increase in the effect level results in a decrease in the response.

Table 5-4: ANOVA for the selected factorial model of ID response

Soruce	Sum of squares	df (degrees of freedom)	Mean square	F-vale	P-value	
Model	4.1E+006	9	4.4E+005	29.68	< 0.0001	significant
A-Conc	*9.7E+005*	*1*	*9.7E+005*	*64.8*	*< 0.0001*	
B-Core.F	*29800.09*	*1*	*29800.09*	*1.9*	*0.1734*	
C-Shell.F	*2.3E+006*	*1*	*2.3E+006*	*159*	*< 0.0001*	
D-Spinning.D	*1.1E+005*	*1*	*1.1E+005*	*7.8*	*0.0105*	
AB	*3203.02*	*1*	*3203.02*	*0.2*	*0.6492*	
AC	*1.3E+005*	*1*	*1 .3E+005*	*9.2*	*0.0060*	
AD	*79278.81*	*1*	*79278.81*	*5.2*	*0.0317*	
BD	*1.6E+005*	*1*	*1.6E+005*	*11.2*	*0.0028*	
ABD	*1.1E+005*	*1*	*1.079E+005*	*7.1*	*0.0138*	
Residual	3.3E+005	22	15056			
Lack of Fit	*4672*	*6*	*778*	*0.4*	*0.8429*	*not significant*
Pure Error	*2.8E+005*	*16*	*1778*			

The F-value is the test for comparing model variance with residual (error) variance. If the variances are similar, the ratio will be close to one, in which case it is likely that none of the factors would have a significant effect on the response. The F-value is obtained by dividing the model mean square by residual mean square. The model F-value of 29.68 implies that the model is significant. There is a 0.01% chance that a lack of fit F-value this large could occur due to noise. Non significant lack of fit is a good result (we want the model to fit).

P-value defines the factors that are significant terms in the model. Each factor must have a P-value less than 0.05 to be considered in the regression model. In this case A, C, D, AC, AD, BD and ABD are significant model terms, because values greater than 0.1000 indicate that the model terms are not significant. By default, Design-Expert considers values of 0.05 as significant model terms. However, this value can be changed from 0.1 to 0.05, depending on how much risk one wishes to accept.

Table 5-5: Additional data from ANOVA (ID)

Std. Dev.	122.71	R-Squared	0.92
Mean	429.13	Adj R-Squared	0.89
C.V. %	28.59	Pred R-Squared	0.83
PRESS	7.008E+005	Adeq Precision	17.25

Standard deviation of 122.7 displays the deviation associated with the experiment. “Mean” is overall average of all the response data.

C.V. (coefficient of variation), C.V. value of 28.6 % indicated that the proportion of variability unexplained by the model was low.

Press value (7.008E+005) is the measure of how the model fits each point in the design.

R-Squared gives a measure of the amount of variation around the mean explained by the model. The model was able to explain more than 91% of the variability in the fiber diameter.

Adjusted R-squared-value of 0.89 indicated that all the selected terms contributed significantly to the model.

Predicted R-squared of 0.84 indicated that the model was able to explain more than 85% of the variability in predicting new observations in the design space.

Adequate precision measures the signal to noise ratio, a ratio greater than 4 is desirable. The ratio of 17 indicates an adequate signal.

Final equation in terms of coded factors (ID):

Inner.D = 429.1 + (174.7*A) + (30.5 * B) + (273.7* C) + (60.6* D) - (10* A*B) + (65.9*A*C) + (49.7*A*D) – (72.8*B*D) – (58*A*B* D) 5.1

Final equation in terms of actual factors (ID):

Inner ID = 15514.9 – (1345.6 * Conc) – (16635.8 * Core.F) – (583 * Shell.F) - (1755 * Spinning.D) + (1431* Conc* Core.F) + (65.9* Conc* Shell.F) + (149.3* Conc* Spinning.D) + (1818.7* Core.F * Spinning.D) – (154.8* Conc * Core.F * Spinning.D) 5.2

Table 5-6 tabulated the actual and predicted response values with the residual for ID response.

Table 5-6: Actual and predicted values of ID response

Run	Actual value	Predicted value	Residual
1	352	396	-44
2	615	485	130
3	564	499	65
4	540	447	93
5	507	507	0
6	1167	943	224
7	1158	1164	-6
8	219	305	-86
9	509	485	24
10	495	681	-186
11	0	-19	19
12	0	-19	19
13	0	2	-2
14	0	2	-2
15	190	91	99
16	0	31	-31
17	0	31	-31
18	400	396	4
19	960	984	-24
20	399	264	135
21	497	506	-9
22	1016	1164	-148
23	1028	984	44
24	0	83	-83
25	417	447	-30
26	0	83	-83
27	872	681	191
28	371	305	66
29	182	83	99
30	417	498	-81
31	0	264	-264
32	849	943	-94

Table 5-7: ANOVA for selected factorial model (OD)

Surces	Sum of squares	df (degrees of freedom)	Mean square	F-value	P-value	
Model	10548	15	703	9.4	< 0.0001	significant
A-Conc	*1484*	*1*	*148*	*19.9*	*0.0004*	
B-Core.F	*289.4*	*1*	*289*	*3.8*	*0.0664*	
C-Shell.F	*6679.9*	*1*	*6680*	*89.5*	*< 0.0001*	
D-Spinning.D	*165.2*	*1*	*165*	*2.2*	*0.1561*	
AB	*45*	*1*	*45*	*0.6*	*0.4486*	
AC	*28.3*	*1*	*28*	*0.3*	*0.5466*	
AD	*129*	*1*	*129*	*1.7*	*0.2069*	
BC	*29.4*	*1*	*29*	*0.3*	*0.5387*	
BD	*596.9*	*1*	*596*	*8*	*0.0121*	
CD	*10.3*	*1*	*10*	*0.1*	*0.7150*	
ABC	*20*	*1*	*20*	*0.2*	*0.6109*	
ABD	*336*	*1*	*336*	*4.5*	*0.0497*	
ACD	*6.8*	*1*	*6.8*	*0*	*0.7657*	
BCD	*211*	*1*	*211*	*2.8*	*0.1117*	
ABCD	*516*	*1*	*516*	*6.9*	*0.0182*	
Pure Error	1193	16	74.5			

The model F-value of 9.43 implies that the model is significant. There is only a 0.01% chance that a Model F-Value this large could occur due to noise. Values of Prop > F less than 0.05 indicate that model terms are significant. In this case A, C, BD, ABD and ABCD are significant model terms. While values greater than 0.1indicate that the model terms are not significant.

A square transformation (Sqrt) was applied as suggested by a Box-Cox plot (see Appendix C, Figure C8). The transformation of the response data was necessary for three reasons: 1) stabilizing response variance, 2) bringing the distribution of the response variable closer to the normal distribution and 3) improving the fit of the model to the data.

Table 5-8: Additional data from ANOVA (OD)

Std. Dev.	8.64	R-Squared	0.89
Mean	28.14	Adj R-Squared	0.80
C.V. %	30.69	Pred R-Squared	0.59
PRESS	4773.51	Adeq Precision	8.58

Standard deviation of 8.64 displays the deviation associated with the experiment. Mean is the overall average of all the response data.

C.V. (coefficient of variation), C.V. value of 30.69 indicated that the proportion of variability unexplained by the model was low.

Press value (4773.51) is the measure of how the model fits each point in the design.

R-Squared gives a measure of the amount of variation around the mean explained by the model. The model was able to explain more than 89 % of the variability in the fiber diameter.

Adjusted R-squared-value of 0.80 indicated that all the selected terms contributed significantly to the model.

Predicted R-squared of 0.60 indicated that the model was able to explain more than 60% of the variability in predicting new observations in the design space.

Adequate precision measure the signal to noise ratio, a ratio greater than 4 is desirable. The ratio of 8.5 indicates an adequate signal.

Final equation in terms of coded factors (OD):

Sqrt(Outer.D) = 28.1 + (6.8*A) + (3*B) + (14.4*C) + (2.2*D) – (1.1*A*B) – (0.9* A*C) + (2*A*D) – (0.9*B*C) – (4.3*B*D) – (0.5*C*D) + (0.7*A*B*C) – (3.2* A*B*D) – (0.4*A*C*D) + (2.5*B*C* D) + (4*A*B*C*D) 5.3

Final equation in terms of actual factors (OD):

Sqrt(Outer.D) = 2588.5 – (215.7*Conc) – (3309.7*Core.F) – (917.4* Shell.F) – (297.3*Spinning.D) + (274.5*Conc*Core.F) + (75.9* Conc* Shell.F) + (24.5* Conc* Spinning.D) + (1212.8*Core.F* Shell.F) + (365.6*Core.F* Spinning.D) + (102.9* Shell.F*Spinning.D) – (98.5*Conc*Core.F*Shell.F) – (30*Conc*Core.F * Spinning.D) – (8.3*Conc*Shell.F*Spinning.D) – (132.4*Core.F*Shell.F* Spinning.D) + (10.7*Conc*Core.F*Shell.F*Spinning.D) 5.4

Table 5-9 tabulated the actual and predicted response values with residual for OD response.

Table 5-9: Actual and predicted values of OD response

Run	Actual value	Sqrt(Outer.D)	Predicted value	Residual
1	745	27	31	-4
2	1683	41	38	2
3	1407	37	36	1
4	1622	40	36	3
5	1736	41	41	0
6	3050	55	52	3
7	2881	53	51	2
8	970	31	32	-1
9	1354	36	38	-2
10	1266	35	42	-7
11	0	0	11	-11
12	0	0	14	-14
13	0	0	0	0
14	0	0	12	-12
15	497.7	22	11	11
16	0	0	0	0
17	0	0	0	0
18	1288	35	31	4
19	2291	47	47	0
20	852	29	14	15
21	1713	41	41	-0
22	2340	48	51	-3
23	2285	47	47	-0
24	0	0	0	0
25	1301	36	36	-0
26	0	0	0	0
27	2458	49	42	7
28	1114	33	32	1
29	637	25	13	12
30	1132	33	37	-3
31	0	0	0	0
32	2456	49	52	-3

5.7 Examination of interaction effects

An interaction takes place when the effect of one factor depends on the level of another factor. In the case of the ID response, it can be seen from the list of effects in Table 5.2 that the interaction effect BD has a higher contribution effect compared to the other main interaction effects. The interaction effect graph is shown in Figure 5.5. The following significant interactions are AC (positive effect), ABD (negative effect) and AD (positive effect), as shown in Figures 5.6 and 5.7, respectively. Since the software does not present graphs in four dimensions, we will only present the two interaction effect graphs for analysis. It is noted that all significant interaction factors contain A (shell concentration), except BD. This is expected as the shell concentration is one of the largest contributing factors.

The I (beam) symbol that appears on the interaction graphs depict the 95% least significant difference (LSD) interval for the plotted points. Those points that have non-overlapping intervals are significantly different.

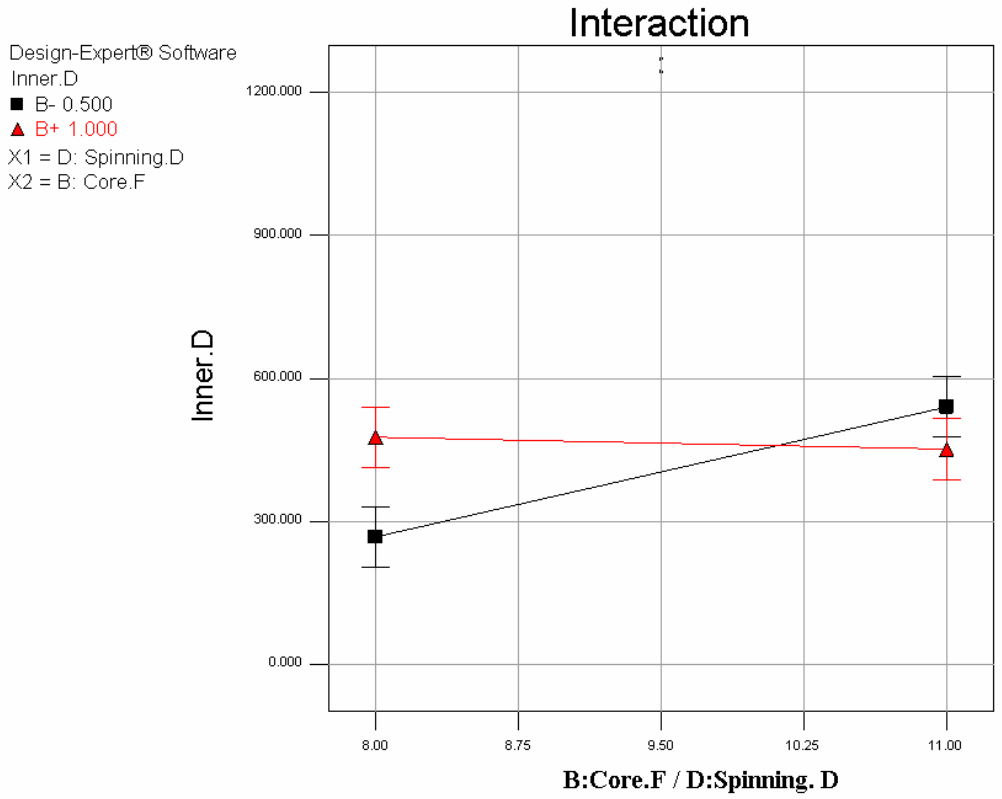

Figure 5.5: Interaction effect between factor B (core feed rate) and D (spinning distance) on fiber ID.

The plot in Figure 5.5 presents the interaction effect of core feed rate and spinning distance. This plot indicates that the core feed rate is less significant at the high spinning distance. The other important interaction effect on fiber ID is AC, as shown in Figure 5.6. The spread of the points is on the right-hand side of this graph where the concentration is larger than the spread between the points on the left-hand side of the graph where the concentration is low. This indicates that the effect of shell feed rate (C) on ID is significant at the high level of polymer solution concentration (A). In other words, higher ID can be obtained by using a high concentration and high shell feed rate (possibly in a limited range).

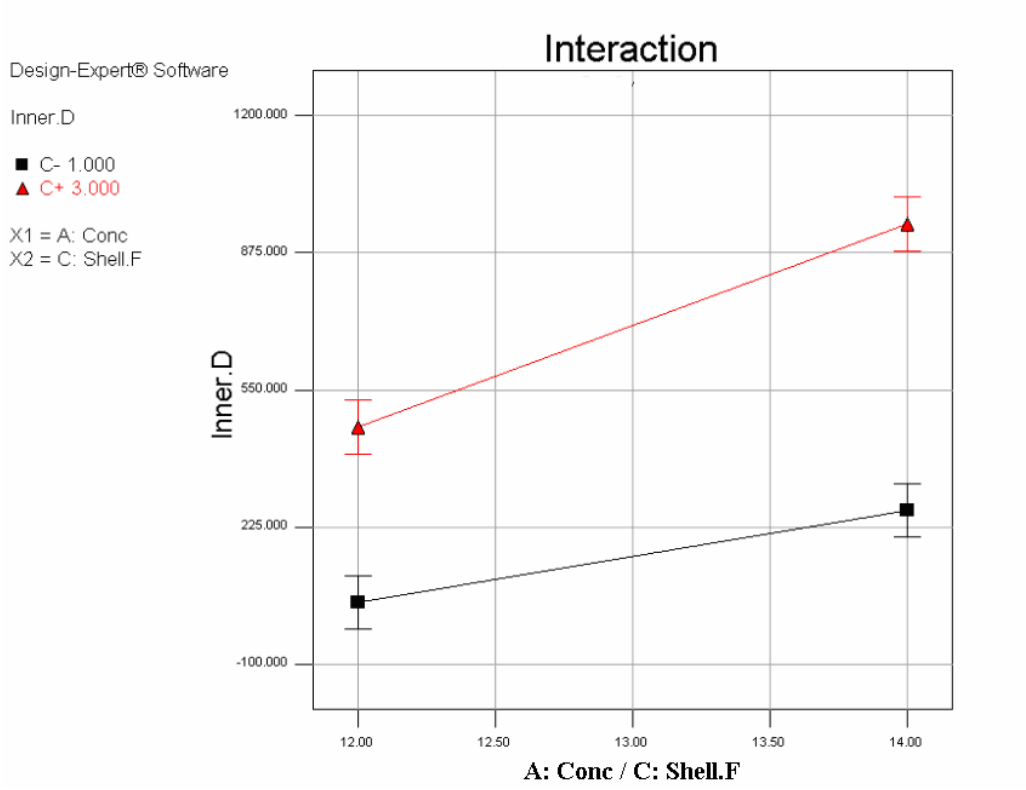

Figure 5.6: Interaction effect between factor A (concentration) and C (shell feed rate) on fiber ID.

The final interaction effect towards ID explored here is AD (the interaction between the spinning distance (D) and concentration (A)). See Figure 5.7. It is clearly seen that the spread of the points on both sides of the graph is small, and that they are

smaller on the left side of the graph where concentration is low. This indicates that spinning distance is only significant at higher polymer solution concentrations.

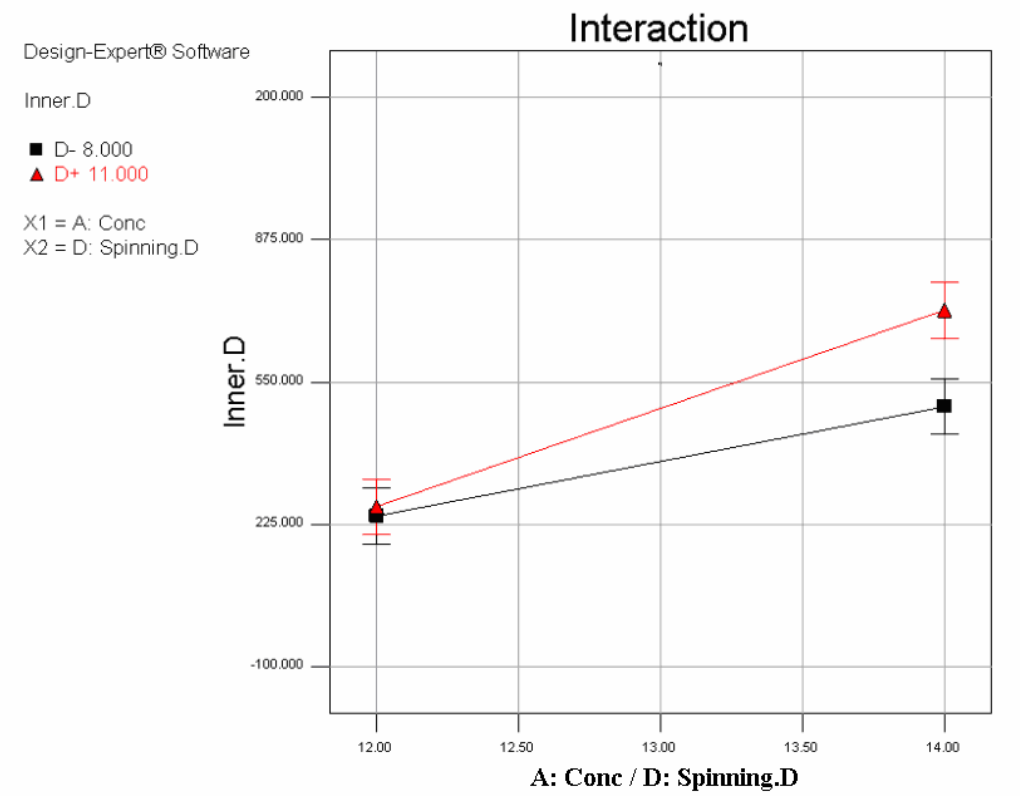

Figure 5.7: Interaction effect between factor A (concentration) and D (spinning distance) on fiber ID.

In the case of the OD response, the list of effects in Table 5.3 shows that the main interaction effect is BD (interaction between core feed rate and spinning distance). It is the prime negative interaction effect and it contributes more towards the OD than all other interaction effects. The following interactions, in decreasing order, are ABCD, ABD, BCD, AD, AB and AC.

The plot in Figure 5.8 presents the interaction effect of BD (the core feed rate and spinning distance) on OD. This plot indicates that the core feed rate is significant at the low spinning distance.

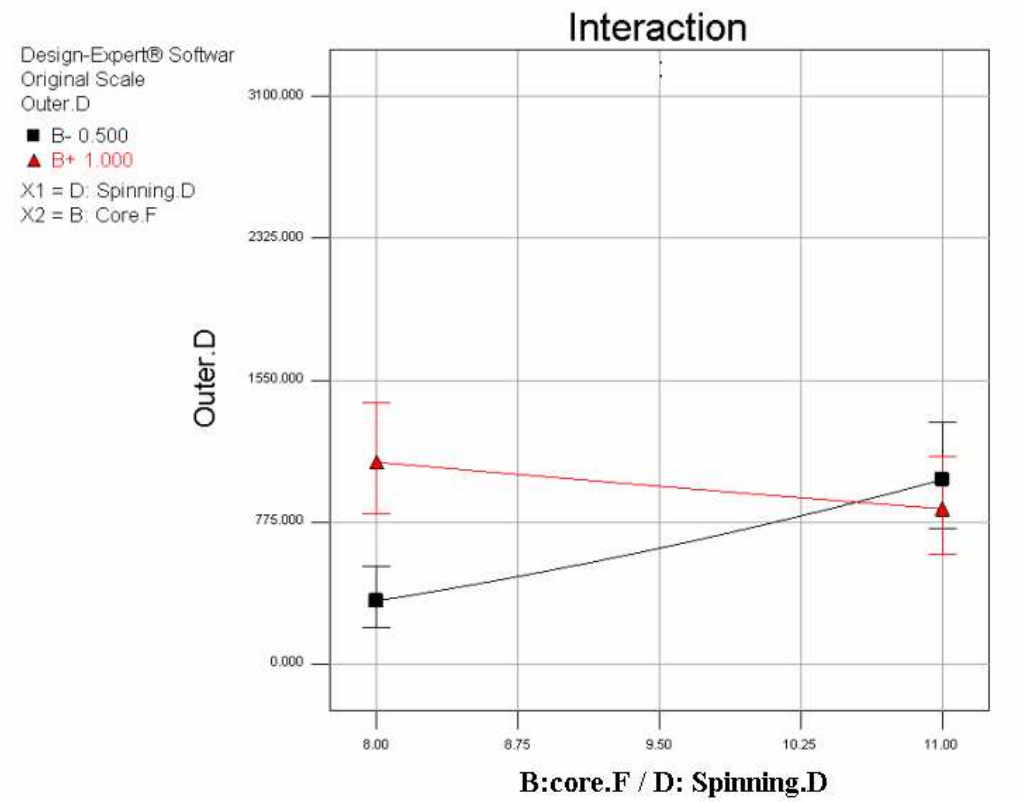

Figure 5.8: Interaction effect between factor B (core feed rate) and D (spinning distance) on OD.

5.8 Cube plots

Cube plots are effective for simultaneously representing the effect of the three factors that create significant effects as a function of the predicted response for the -1 and +1 levels [77], as shown in Figures 5.9 and 5.10.

The plot in figure 5.9 shows how the three factors combine to affect the response. All values shown are predicted values, thus allowing plots to be made even where there are missing actual data. The factors that are of interest in Figure 5.9 are A, C and D. The ID is high at the A+, D+, C+ settings (top back right corner), with a predicted response of over 105, which corresponds to an increase in shell feed rate.

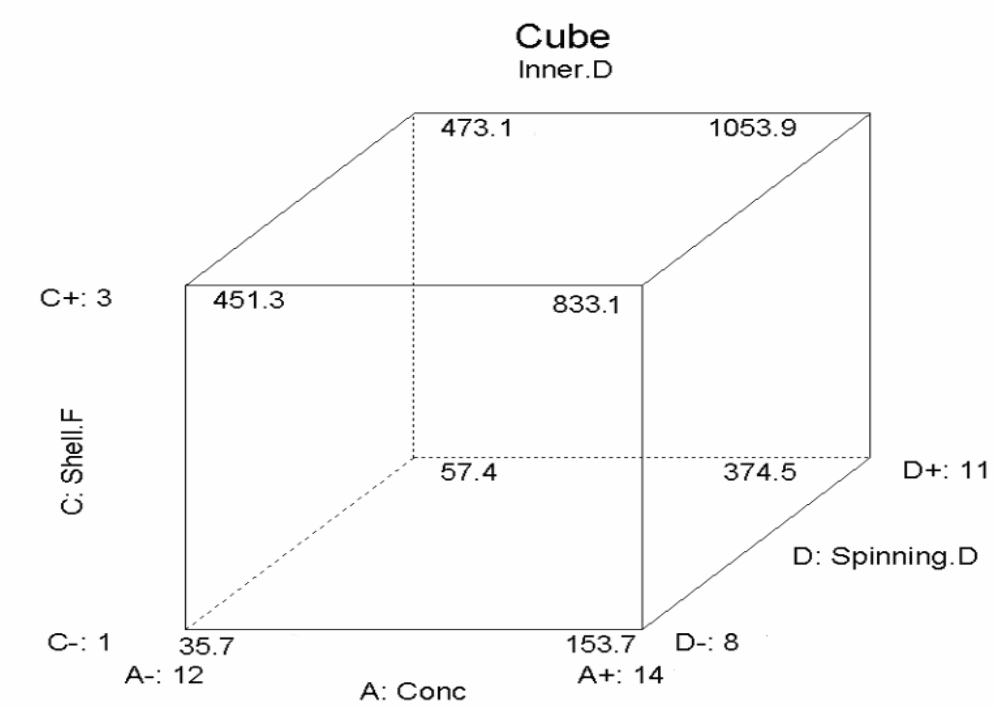

Figure 5.9: Cube plot of A, B and C with ID response.

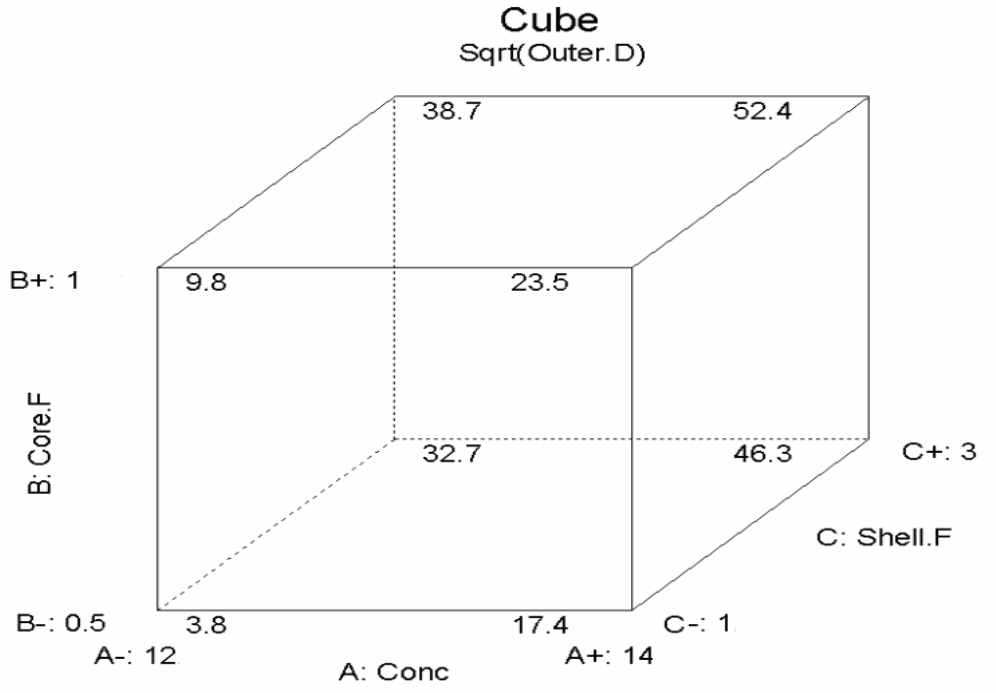

Figure 5.10: Cube plot of A, B and C with OD response.

In the plot shown in figure 5.1 the OD is high at the A+, C+, D+ settings (top back right corner), with a predicted response of over 52.4, which corresponds to an increase in core feed rate .

5. 9 3D plots of the interaction

The last feature explored here is the 3 D surface model, which provides a clearer view of the interaction effect that creates significant effects as function of the response.

The plot in Figure 5.11 presents the interaction graph of shell feed rate and polymer concentration. This plot indicates that high ID can be achieved by using the high shell feed rate and increasing the polymer concentration (possibly in a limited range).

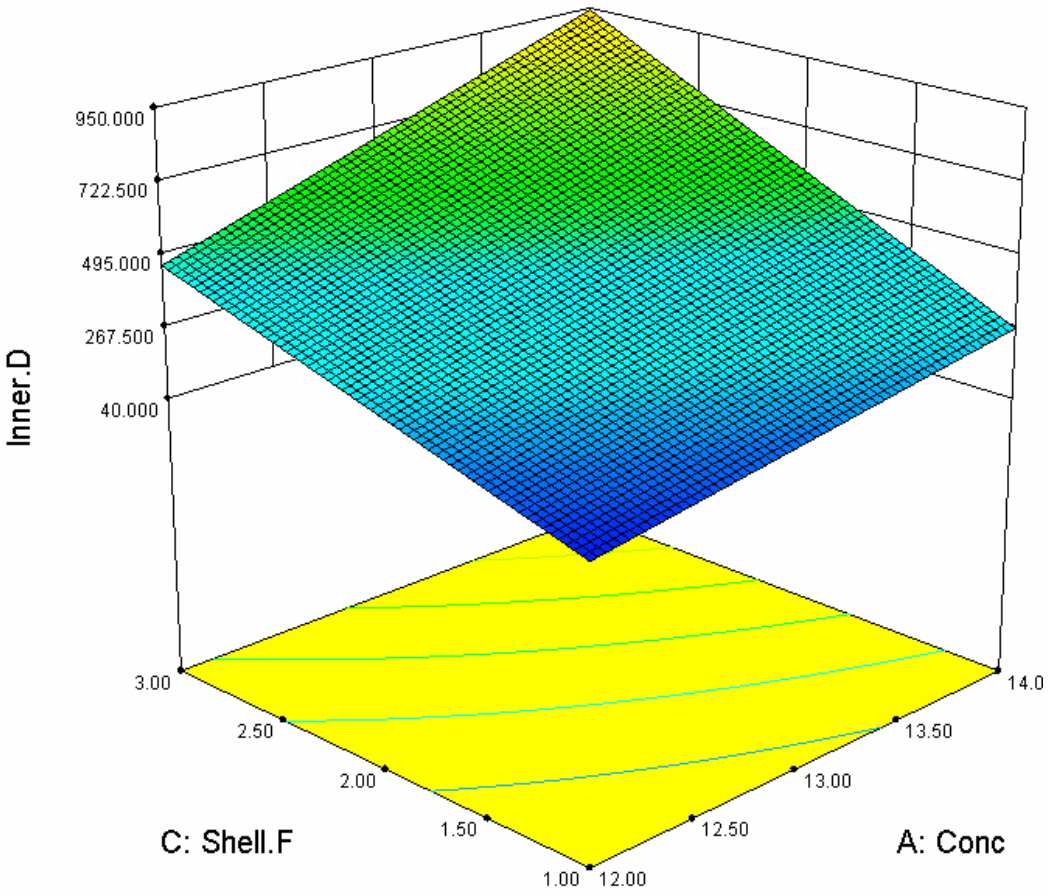

Figure 5.11: 3D view of the AC interaction on the ID response.

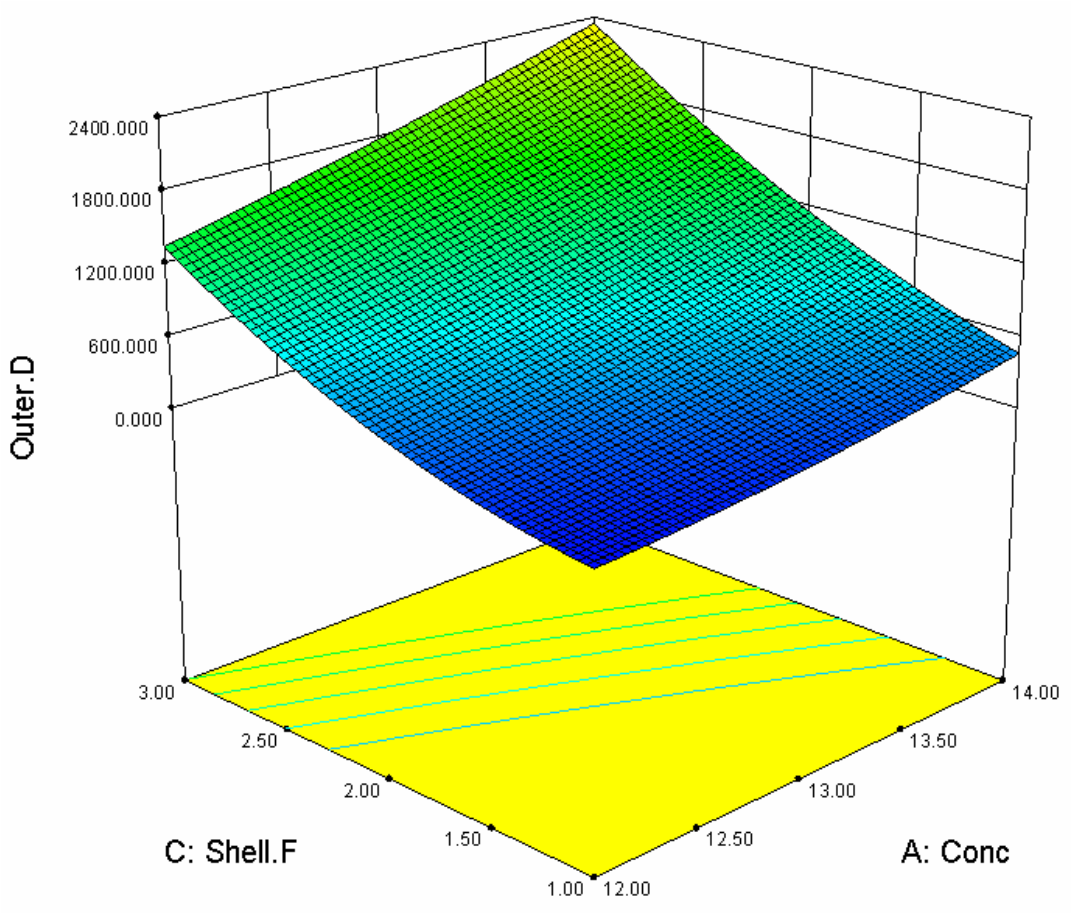

Figure 5.12: 3D view of the AC interaction on the OD response.

In the plot in Figure 5.12, it is clear that a high OD can be achieved by using a high shell feed rate and increasing the polymer concentration (possibly in a limited range).

5.10 Summary

It can be concluded that shell feed rate is the most dominant factor influencing the ID and OD of electrospun fibers. Setting the shell feed rate high is the key parameter. From a half-normal plot of the factor effects of the model, one can see that the dominant effects in decreasing order are: shell feed rate, shell solution concentration, spinning distance and core feed rate. The shell feed rate and shell

solution concentration contribute more than all other factors towards the ID and OD values of the fibers and therefore are the most important parameters. The most important interaction effects are as follow: in the case of ID the highest significant interaction effects on ID are BD [core feed rate and spinning distance], and AC [concentration and shell feed rate]. In the case of OD, besides the BD, AB, AD and AC interaction effects, there are three and four-interaction effects involved. These interaction effects are ABCD and ABD respectively. It is noted that most of the interactions contain factor A (concentration). This is expected, as the polymer solution concentration is one of two major contributing factors that significantly affect the ID and OD of the fibres. The core feed rate, as an independent factor, has a less significant effect towards the ID and OD of the electrospun fibres.

The results of the factorial design experiments (Table 5-1) indicated that the preferable electrospinning conditions for electrospinning of CA hollow fibres using coaxial spinnerets having internal diameters of 0.3 mm and 1.2 mm for the core and shell needles respectively, with gap space separating the core and shell needles of 0.3 mm (see Appendix E, Figure E1 for the specific mechanical design) involved using a high polymer concentration (14 wt %), low core feed rate (0.5 ml/hr), high shell feed rate (3 ml/hr) and a small spinning distance (8 cm).

Chapter 6

Conclusions and Recommendations

6.1 Co-electrospinning

In this study, coaxial capillary spinnerets capable of generating hollow nanofibers were successfully designed. This involved using two immiscible fluids. Cellulose acetate in acetone:dioxane as the shell fluid, and mineral oil as the core fluid, were introduced to the shell and core capillary, respectively, at controlled feed rates. The electrospun CA nanofibers were well aligned using a collection water bath. TEM images clearly indicated formation of a core-shell structure with oil as core and CA as shell. In order to make the fibers hollow the electrospun fibers were immersed in octane over a period of 24 hr. SEM images of cross- sections of the hollow fibers showed that the core was completely removed from the fibers. The resulting hollow fiber had ID and OD values ranging from 182 nm to 1 µm and 500 nm to 3 µm, respectively. These results showed that the diameter of these fibers is smaller than that of fibers produced by conventional spinning.

Important parameters and their effects were studied: (a) system parameters include polymer concentration, type of solvent, solvent ratio, dynamic viscosity, solution conductivity and solution surface tension (b) process variables involve the core and shell feed rate, spinning distance and voltage applied; and (c) ambient parameters involves humidity.

6.2 Factorial design of experiments

A full factorial design with two replications was used to determine the effects of the selected factors on the two responses variables, namely ID and OD of the electrospun fiber. The most powerful effects in decreasing order are: shell feed rate, shell solution concentration, spinning distance and core feed rate. The shell feed rate and CA concentration contribute more than all other factors towards the ID and OD of the fibers and are therefore the most important parameters. The most important two interaction effects are the interaction between shell feed rate and concentration, and the interaction between concentration and spinning distance. Core feed rate, as an independent variable, has a less significant effect on both ID and OD compared to the other main effects.

6.3 Preferable conditions

A stable electrospinning jet was the key factor that characterized the optimum conditions of the electrospinning process. The optimal spinning conditions for electrospinning of CA hollow fibers in acetone/dioxane are tabulated in the Table 6-1. These conditions were established according to visual observation for the behaviour of the electrospun jet and the morphology and the structure of the electrospun fibers as determined by SEM.

Table 6-1: Preferable conditions established for production of hollow fibers by co-electrospinning of CA

System and process parameters	**Preferable conditions**
Polymer solution concentration	14 wt %
Core feed rate	0.5 ml/hr
Shell feed rate	3 ml/hr
Solvent ratio (acetone:dioxane)	2:1 v/v
Voltage supply	15 kV
Tip to the needle distance	8 cm
Relative humidity	40-50 %
Core spinneret inside diameter	0.3 mm
Shell spinneret inside diameter	1.2 mm
Shell/core gap space	0.3 mm

6.4 Recommendations for future work

1. Most of the SEM images of electrospun CA fibers revealed that the fibers (from any particular experiment) are slightly different in size. The reason for this is unclear, and requires further investigation.

2. Alignment of CA fibers was achieved by electrospinning into a water bath. The electrospun fibers were then drawn from over the surface of the water to a small rotating drum. A scale up continuous aligned nanofibers yarn process for model fabrication is still not available.

3. An important characteristic of electrospun nanofibers are their small diameters ranging from nanometres to a few micrometers. Handling, mounting, cutting and exposing the cross- section of these fibers is still a difficult issue.

4. Little research has been done on electrospun fibers in terms of characterization of the alignment of the fibers. Characterization of hollow nanofibers should include diameter distribution, pore size, and mechanical properties like strength, toughness, elongation, and physical properties like tensile strength and elasticity. Procedures have to be developed to determine all these properties of the electrospun hollow nanofibers in a response model. A further step could be to compare the properties of hollow nanofibers to the fibers manufactured by conventional spinning.

5. Some degree of hardness (rigidity) is still required in the walls of CA hollow fibers as some of the hollow fibers tend to collapse after the removal of the core. Hence, investigation into the preparation of hollow fibers with a rigid wall should be included in future work.

6. Determining the usability of the electrospun CA hollow fiber membranes for water treatment should also receive attention. That might include: Determination of the effect that fiber wall diameter has on transport properties in the hollow fiber assemblies. How does this affect the hollow

fiber membranes separation performance? Determination of hollow nanofibers properties such as flux rate, permeability and selectivity.

7. Other potential focus areas include, investigating different collector devices and methods to extract the electrospun nanofibers from the collector, varying the process parameters to obtain thick nanofibers, and utilizing other solvents to dilute the solution for a possible reduction in the solvents volatility.

8. A next generation of co-electrospinning apparatus should include capabilities of digital controlling the temperature, humidity and the electrospinning distance (the distance between the spinneret and the collector) during the electrospinning process.

References

1. Qin X.,Wang S., Filtration properties of electrospinning nanofibers. Applied Polymer Science 2006, 102(2): 1285-1290.
2. Han S., Son W., Youk J., Lee T., Park W., Ultrafine porous fibers electrospun from cellulose triacetate. Materials Letters 2005, 59(24-25): 2998-3001.
3. Gopala R., Kaur S., Ma Z., Chan C., Ramakrishna S., Matsuura T., Electrospun nanofibrous filtration membrane. Membrane Science 2006, 281 (1-2): 581-586.
4. Barhatea R., Loonga C., Preparation and characterization of nanofibrous filtering media. Membrane Science 2006, 283(1-2): 209-218.
5. Qin J., Li Y., Lee L., Lee H., Cellulose acetate hollow fiber ultrafiltration membranes made from CA/PVP 360 K/NMP/water. Membrane Science 2003, 218 (1): 173-183.
6. Mohan, A., MSc, thesis. Formation and characterization of electrospun nonwoven webs. North Carolina State University, 2002.
7. Fiber spinning machine incorporates nanoparticles in fiber bulk http://www.empa.ch/plugin/template/empa/*/22295, [10 May 2008].
8. Formhals, Electrospinning, in US Patent. 1934, 1975504: USA.
9. Gupta P., PhD thesis. Processing-structure-property studies, Virginia Polytechic Institute and State University, 2004.
10. Moon S., Farris R., How is it possible to produce highly oriented yarns of electrospun fibers. Polymer Engineering & Science 2007, 47(40): 1530-1535.
11. Ramakrishna S., Teo W., A review on electrospinning design and nanofibers assemblies. Nanotechnology 2006, 17 (14): 89-106.
12. McCann J.T., Li D., Xia Y., Electrospinning of nanofibers with core-sheath, hollow, or porous structures. Materials Chemistry 2005, 15(7): 735-738.
13. Young D. M.Sc thesis. Hyaluronic acid-based nanofibers via electrospinning. North Carolina State University, 2006.
14. Son W., Youk J., Lee S., Park W., Effect of pH on electrospinning of poly (vinyl alcohol). Materials Letters 2005, 59(12): 1571-1575.
15. Reneker., Yarin A., Electrospinning jets and polymer nanofibers. Polymer 2008, 48(10): 2387-2425.

16. Ramakrishna S., Lim T., Fujihara K., Teo W., Zuwei, An introduction to electrospinning and nanofibers. 2005, chapter 3.
17. Mueller J., Free Mind software, 2004 (8).
18. Queen, H., MSc thesis. Electrospinning chitosan-based nanofibers for biomedical applications, North Carolina State University, 2006.
19. Swart, M., MSc, thesis. Synthesis and characterization of electrospun organic-inorganic hybrid graft copolymer nanofibers of poly(methyl methacrylate) and polydimethylsiloxane, University of Stellenbosch, 2007.
20. Subbiah T., Bhat G., Tock R., Parameswaran S., Ramkumar S.,Electrospinning of nanofibers. Applied Polymer Science 2004, 96(2):557-569.
21. Wikipedia, the free encyclopedia, http://en.wikipedia.org/wiki/Surface_tension, [26 July 2008].
22. Du J., Shintay S., and Zhang Xi., Diameter control of electrospun polyacrylonitrile/iron acetylacetonate ultrafine nanofibers. Polymer Science, Part B 2008, 46(15):1611-1618.
23. Li D., Babel A., Jenekhe S., Xia Y., Nanofibers of conjugated polymers prepared by electrospinning with a two-capillary spinneret. Advanced Materials 2004, 16(22): 2062-2066.
24. Herrera J., Barrero A., Lopezc A., Loscertales G., Marqueze M., Coaxial jets generated from electride Taylor cone scaling laws. Aerosol Science 2003, 34(5):535-552.
25. Jiang H., Hun Y., Li Y., Zhao P., Zhu K., Chen W., A facile technique to prepare biodegradable coaxial electrospun nanofibers for controlled release of bioactive agents. Controlled Release 2005, 108(2-3): 237-243.
26. Jalili R., Hosseini S., Morshed M., The effects of operating parameters on the morphology of electrospun polyacrylonitrile nanofibers. Iranian Polymer 2005, 14(12): 1074-1081.
27. Panda P., Ramakrishna S., Electrospinning of alumina nanofibers using different precursors. Master 2007, 42(6): 2189-2193.
28. Zhang Y., Wang X., Feng Y., Li J., Lim C., Ramakrishna S., Coaxial electrospinning of (Fluorescein isothiocyanate-conjugated bovine serum albumin)-encapsulated poly (E-caprolactone) nanofibers for sustained release. Biomacromolecules 2006, 7(4): 1049-1059.

29. Wannatong L., Sirivat A., Suaphol P., Effects of solvents on electrospun polymeric fibers: preliminary study on polystyrene. Polymer International 2004, 53(11): 1851-1859.
30. Jeun J., Kim Y., Lim Y., Choi J., Jung C., Kang P., Nho Y., Electrospinning of poly (L-lactide-co-D, L-lactide). Industrial & Engineering Chemistry 2007, 13(4): 592-596.
31. Dong D., Nyame V., Macdlarnd A., Wayne E. Jones, W., Polyaniline/Poly (methyl methacrylate) coaxial fibers: The fabrication and effects of the solution properties on the morphology of electrospun core fibers. Polymer Physics 2004, 42(21): 3934-3942.
32. Yim K., Shivkumar S., Effect of molecular weight on fibrous PVA produced by electrospinning. Materials Letters 2004, 58(3-4): 493-497.
33. Gopal R., Kaur S., Ma Z., Chan C., Ramakrishna S., Matsuura T. Electrospun nanofibrous filtration membrane. Membrane Science, 2006, 281(1-2): 581-586.
34. Fridrikh S., Yu J., Brenner M., Rutledge G., Controlling the fiber diameter during electrospinning. Physical Review Letters 2003, 90(14).
35. He J., Liu H., Variational approach to nonlinear problems and a review on mathematical model of electrospinning. Nonlinear Analysis 2005, 63(5-7): 919-929.
36. Shin Y., Hohman M., Brenner M., Rutledge G., Electrospinning: A whipping fluid jet generates submicron polymer fibers. Applied Physics Letters 2001, 78(8):1149-1151.
37. Yang, H., Fabrication and characterization of multifunctional nanofiber nanocomposite structures through co-electrospinning process. Materials Science and Engineering 2007, Drexel University Philadelphia, USA.
38. He J., Wu Y., Zuo W., Critical length of straight jet in electrospinning. Polymer 2005, 46:12637-12640.
39. Spivak A., Dzenis Y., Asymptotic decay of radius of a weakly conductive viscous jet. Applied Physics Letters 1998, 73(21): 3067-3069.
40. Baumgarten P., Electrostatic spinning of acrylic microfibers. Colloid and Interface Science 1971, 36: 71-79.

41. Jiang H., Hun Y., Li Y., Zhao P., Zhu K., Chen W., A facile technique to prepare biodegradable coaxial electrospun nanofibers for controlled release of bioactive agents. Controlled Release 2005, 108(2-3): 237-243.
42. Zussman E., Yarin A., Bazilevsky A., Avrahami R., Feldman M., Electrospun polyacrylonitrile/poly(methyl methacrylate)-derived turbostratic carbon micro-/nanotubes. Advanced Materials 2006, 18(3): 348-535.
43. Dror Y., Salalha W., Avrahami R., Zussman E., Yarin A., Dersch R., Greiner A., Wendorff J., One-step production of polymeric microtubes by co-electrospinning. Small 2007, 3(6): 1064-1073.
44. Songa T., Zhangb Y., Zhoua T., Limb C., Ramakrishnab S., Liua B., Encapsulation of self-assembled FePt magnetic nanoparticles in PCL nanofibers by coaxial electrospinning. Chemical Physics Letters 2005, 415(4-6): 317-322.
45. Wang M., Jing N., Su C, Kameoka J., Electrospinning of silica nanochannels for single molecule detection. Applied Physics Letters 2006, 88: 1-3.
46. Han X., Huang Z., He C., Liu L., Wu Q., Coaxial electrospinning of PC(shell)/PU(core) composite nanofibers for textile application. Polymer Composites 2008, 29(5): 579-584.
47. Gupta B., King M., Hudson S., Loboa E., Hufenus R., Gluck J., Moghe A., Electrospun core-sheath fibers for soft tissue engineering. NTC Project 2006, F05-NS04.
48. Diaz J., Nieves A., Barrero A., Marquez M., Loscertales I., Fabrication of structured micro and nanofibers by coaxial electrospinning. Physics 2008, 127: (012008).
49. Li D., Xia Y., Direct fabrication of composites and ceramic hollow nanofibers by electrospinning. Nano Letters 2004, 4(5): 933-938.
50. Srivastava Y., Loscertales E., Electrospinning of hollow and core/sheath nanofibers using a microfluidic manifold. Microfluidics and Nanofluidics 2008, 4(3): 245-250.
51. Liao I., Chew S., Leong K., Aligned core-shell nanofibers delivering bioactive proteins. Nanomedicine 2006, 1(4): 465-471.
52. Li D., McCann J., Xia Y., Use of electrospinning to directly fabricate hollow nanofibers with functionalized inner and outer surfaces. Small 2005, 1(1): 83-86.

53. Lallave M., Bedia J., Ruiz-Rosas R., Rodríguez-Mirasol J., Cordero T., Otero J., Marquez M., Barrero A., Loscertales I., Filled and hollow carbon nanofibers by coaxial electrospinning of Alcell lignin without binder polymers. Advanced Materials 2007, 19(23): 4292-4296.

54. Bazilevsky A., Yairn A., Megaridis C., Co-electrospinning of core-shell fibers using a single-nozzle technique. Langmuir 2007, 23: 2311-2314.

55. Yee F., Hollow fiber membranes, http://www.cheresources.com/hmembranes.shtml, [10 March 2008].

56. KMS. http://www.kochmembrane.com/index.html, [25 July 2008].

57. Moghe A., Gupta G., Coaxial electrospinning of nanofibers structures: preparation and applications. Polymer Reviews 2008, 48(2): 353-377.

58. Huanga Z., Zhangb Y., Kotakic M., Ramakrishna S., A review on polymer nanofibers by electrospinning and their applications in nanocomposites. Composites Science and Technology 2003, 63(15): 2223-2231.

59. Tungprapa S., Puangparn T., Weerasombut M., Jangchud I., Fakum P., Semongkhol S., Meechaisue C., Supaphol P., Electrospun cellulose acetate fibers: effect of solvent system on morphology and fiber diameter. Cellulose 2007, 14(6): 563-575.

60. Zuwei Maa Z., Kotakia M., Ramakrishna S., Electrospun cellulose nanofibers as affinity membranes. Membrane Science 2005, 265(1-2):115-123.

61 Subramamnian R.S., Non-Newtonianflows, http://www.clarkson.edu/subramanian/ch301/notes/nonnewtonian.pdf, [12 July 2008].

62. Gomez-diaz D., Navaza J.M., Guintans-Riverio L.C., Influence of concentration and temperature upon Rheology of carrageen aqueous solutions,http://ejeafche.uvigo.es/index.php?option=com_docman&task=doc_view&gid=77, [10 September 2008].

63 Ko F., Gogotsi Y., Ali A., Naguib N., Ye H., Yang G.L., Li C., Willis P., Electrospinning of continuous carbon nanotube-filled nanofiber yarns. Advanced Materials 2003, 15(14): 1161-1165.

64. Pan H., Li L., Hu L., Cui X., Continuous aligned polymer fibers produced by a modified electrospinning method. Polymer 2006, 47: 4901-4904.

65. Katta P., Alessandro M., Ramsier R., Chase G., Continuous electrospinning of aligned polymer nanofibers onto a wire drum collector. Nano Letters 2004, 4(11): 2215-2218.
66. Ishii Y., Sakai H., Murata H., A new electrospinning method to control the number and diameter of uniaxially aligned polymer fibers. Materials Letters 2008, 62(19): 3370-3372.
67. Li D., Wang Y., Xia Y., Electrospinning nanofibers as uniaxially aligned arrays and layer-by-layer stacked films. Advanced Materials 2004, 16(4): 361-366.
68. Smit E., Buttner U., Sanderson R.D., Continuous yarns from electrospun fibers. Polymer 2005, 46(8): 2419-2423.
69. Wikipedia, the free encyclopedia. http://en.wikipedia.org/wiki/Microtome, [15 September 2008].
70. Microsectioning plus optical and scanning electron microscopy. http://www.soldertec.com, [22 May 2008].
71. Gluck M.J., MSc thesis. Electrospun nanofibrous poly(e-caprolactone) (PCL) scaffolds for liver tissue engineering, North Carolina State University ,2007.
72. Sigmund W., Yuh J., Park H., Maneeratana V., Pyrgiotakis G., Daga, A., Taylor J., Nino J., Processing and structure relationships in electrospinning of ceramic fiber systems. The American Ceramic Society 2006, 89(2): 395-407.
73. Fong H., Chun I., Reneker D., Beaded nanofibers formed during electrospinning. Polymer 1998, 40: 4585-4592.
74. Sun B., Duan B., Yuan X., Preparation of core/shell PVP/PLA ultrafine fibers by coaxial electrospinning. Applied Polymer Science 2006, 102(1): 39-45.
75. Srinivasarao M., Collings D., Philips A., Patel S., Three-dimensionally ordered array of air bubbles in a polymer film. Science 2001, 292(5514): 79-83.
76. Li D., Xia Y., Electrospinning of nanofibers: Reinventing the wheel. Advanced Materials 2004, 16(14), 1151-1170.
77. Design Expert, statistical software, State-Ease, USA, 2008 (v.7).
78. Wiley, Design and analysis of experiments, 6th Edition, ISBN: 978-0-471-48735-7, 2004, chapter 2.

Appendix

A.1 Project resources

A.1.1 Project partners

The project partner (Department of Chemistry & Polymer Science) was responsible for:

1. project management, including budgetary and control of all funds
2. providing chemicals, solvents and laboratory.

A.1.2 Computer hardware and software

- SEM-fiber diameter analysis software
- Design expert software (v 7)
- Inventor 9 software
- Gantt chart software (Smart Draw) (v 1)
- Free mind software (v 2)
- Google Sketch up (v 7)

A.2 Solutions preparation

The volume of solution required for electrospinning was at least 20 ml.
The solvents considered were acetone, dimethylacetamide, dioxane, methanol, acetic acid, ethanol, water and ethylene chloride.
Table A.2 shows the physical properties of solvents used in this study.

Table A1: Properties of solvents used in this study

Solvent	Density (g/ml)	Boiling point (^{o}C) at 1 atm
Acetone	0.780	56.2
Dioxane	1.033	101.1
Methanol	0.790	64.7
Dimethylacetamide	0.940	164
Acetic acid	1.049	118.1
Ethanol	0.780	78.0
Ethylene chloride	1.250	83.0

The following calculation was carried out to determine the weight of the polymer and solvent

e.g. 30 ml polymer solution, 2:1 solvent ratio and 12 wt % solution concentrations

Total volume 30 ml = 20 ml main solvent + 10 ml co-solvent

Total solvent mass (g) = main solvent mass (ρ) * (20 ml) + co-solvent mass (ρ) * (10 ml)

So we can get:

12 wt % = Polymer mass/ (polymer mass + solvent mass)

Polymer mass (g) = (solvent mass * 12/100) / 0.88

All the solutions were stirred on a magnetic stirrer plate for 24 hours at room temperature until the solutions became homogeneous, and then the container with the solution was sealed and stored at room temperature until use. Some changes in the viscosity of the solution were visible after a period of 72 hr.

A.3 Example of calculating standard deviation

$$s = \sqrt{\frac{\sum\left(x - \bar{x}\right)^2}{N}}$$

where

S = the standard deviation

x = each value in the sample

$\bar{x}$ = the mean of the values

N = the number of values

Here are the average fibers diameter measurements of the two SEM images respectively 882.8 and 852.5 nm

$\bar{x}$ = 867.6

Calculate x-$\bar{x}$

$\sum \left(x - \bar{x}\right)^2$ = 456.6

$$S = \frac{\sqrt{\sum\left(x - \bar{x}\right)^2}}{N} = \sqrt{\frac{456.6}{n}} = 15$$

The standard deviation for the fibers diameter measurements of the two images is 15

B.1 Solution viscosity measurement

Table B1: a and b values of CA (15, 14, 12 and 11 wt %)

Ostwald I
=========

Result Data Series:
CA 15% wt AC/Dioxane 2:1 24/04/2008 1 [Ostwald I]
<T2>

Ostwald: $y = a \cdot x^b$
$\ln(y) = \ln(a) + b \cdot \ln(x)$

ANALYSIS RESULTS:
Number of Input Data Points : 17
Number of Output Data Points : 17

Regression Parameter a : 26.457
Regression Parameter b : 0.79227
Correlation Ratio R : 0.99941
Correlation Ratio R^2 : 0.99883
Standard Deviation s(n-1) : 9.3395 Pa relating to tau

Herschel-Bulkley I
==================

Result Data Series:
CA 15% wt AC/Dioxane 2:1 24/04/2008 1 [Herschel-Bulkley I]
<T2>

Herschel-Bulkley: $y = a + b \cdot x^p$

ANALYSIS RESULTS:
Number of Input Data Points : 17
Number of Output Data Points : 17

Regression Parameter a : 1.1419
Regression Parameter b : 25.862
Regression Parameter p : 0.79764
Correlation Ratio R_xy : 0.99932
Correlation Ratio R_xlog(y) : 0.99978
Standard Deviation s(n-1) : 10.083 Pa relating to tau

Yield Stress tau0 : 1.1419 Pa

Flow Curve

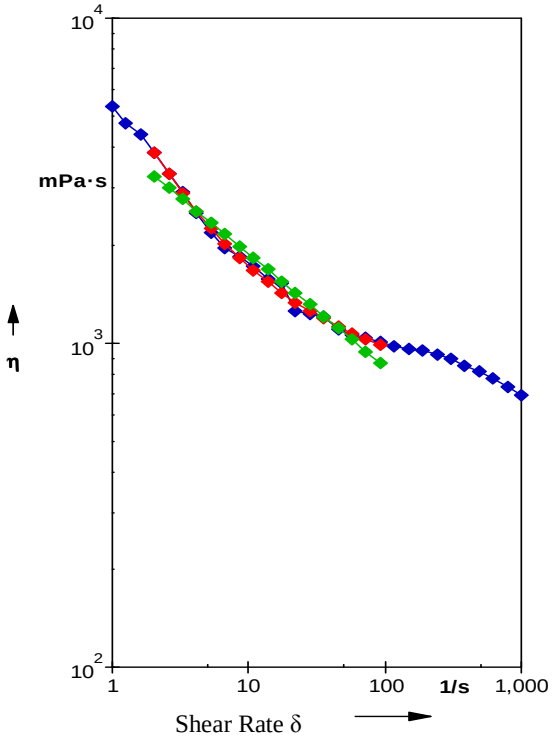

CA 11% wt AC/Dioxan 2:1 28/05/2008 2

CP50-1/TG-SN6634; d=0.048 mm

η Viscosity

CA 11% wt AC/Dioxan 2:1 28/05/2008 2 [Herschel-Bulkley I]

tau0 = 4.7598 Pa; b = 1.6685; p = 0.87064

η Viscosity

CA 11% wt AC/Dioxan 2:1 28/05/2008 2 [Ostwald I]

a = 4.1867; b = 0.6516

η Viscosity

Anton Paar

Anton Paar GmbH

Flow Curve

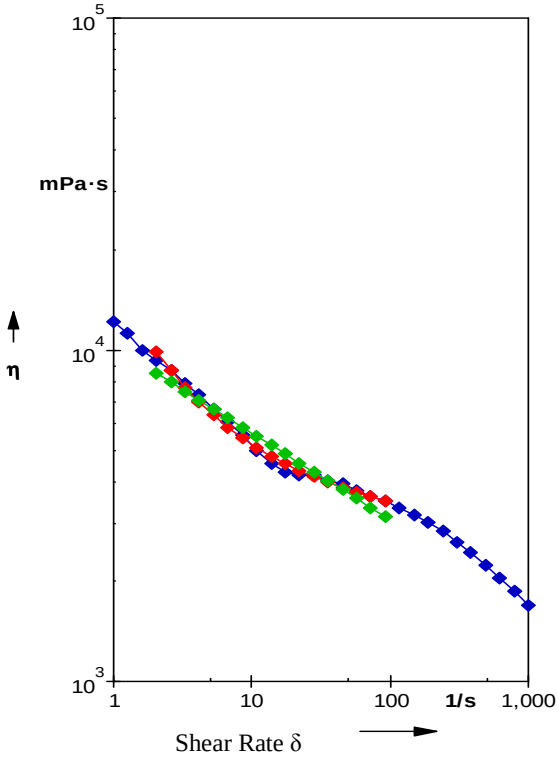

CA 12% wt AC/Dioxan 2:1 10/04/2008 2

CP50-1/TG-SN6634; d=0.048 mm

η Viscosity

CA 12% wt AC/Dioxan 2:1 10/04/2008 2 [Herschel-Bulkley I]

tau0 = 10.261 Pa; b = 5.1204; p = 0.90801

η Viscosity

CA 12% wt AC/Dioxan 2:1 10/04/2008 2 [Ostwald I]

a = 10.193; b = 0.73992

η Viscosity

Anton Paar

Anton Paar GmbH

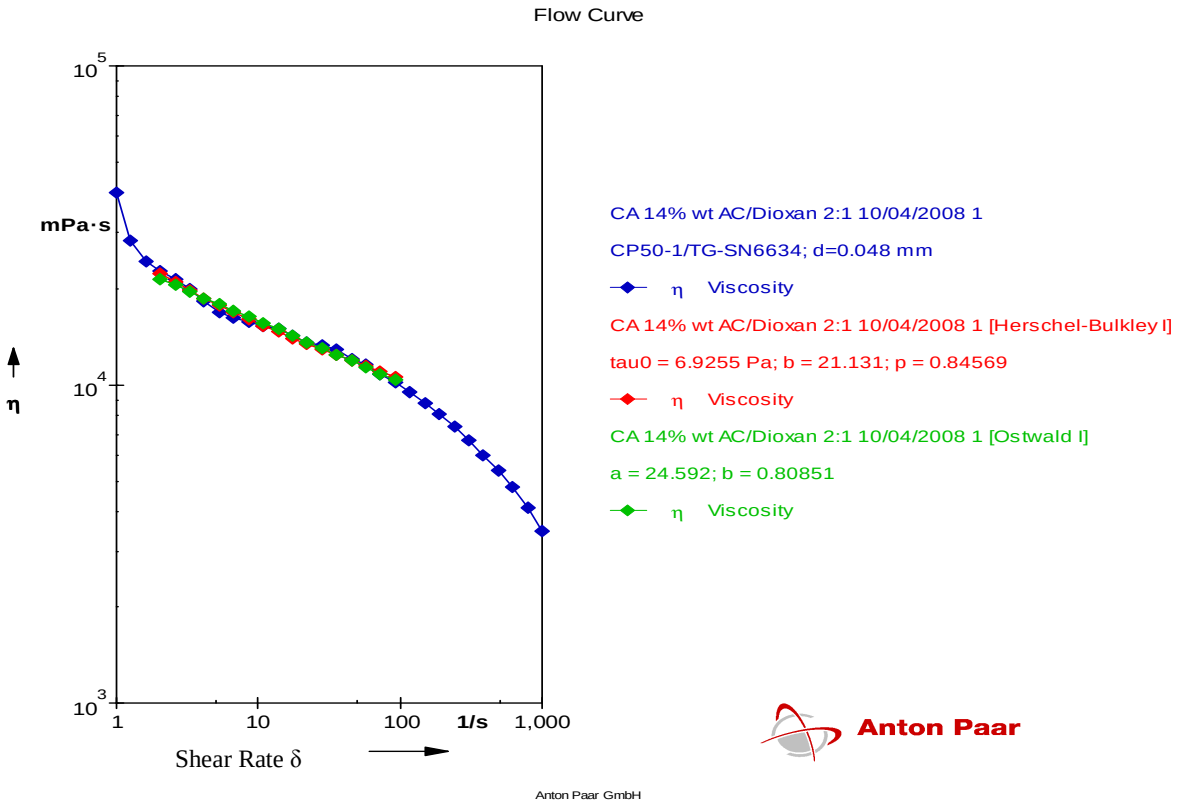
Flow Curve
10^5
mPa·s
η
10^4
10^3
1
10
100
1/s
1,000
Shear Rate δ
CA 14% wt AC/Dioxan 2:1 10/04/2008 1
CP50-1/TG-SN6634; d=0.048 mm
η Viscosity
CA 14% wt AC/Dioxan 2:1 10/04/2008 1 [Herschel-Bulkley I]
tau0 = 6.9255 Pa; b = 21.131; p = 0.84569
η Viscosity
CA 14% wt AC/Dioxan 2:1 10/04/2008 1 [Ostwald I]
a = 24.592; b = 0.80851
η Viscosity
Anton Paar
Anton Paar GmbH

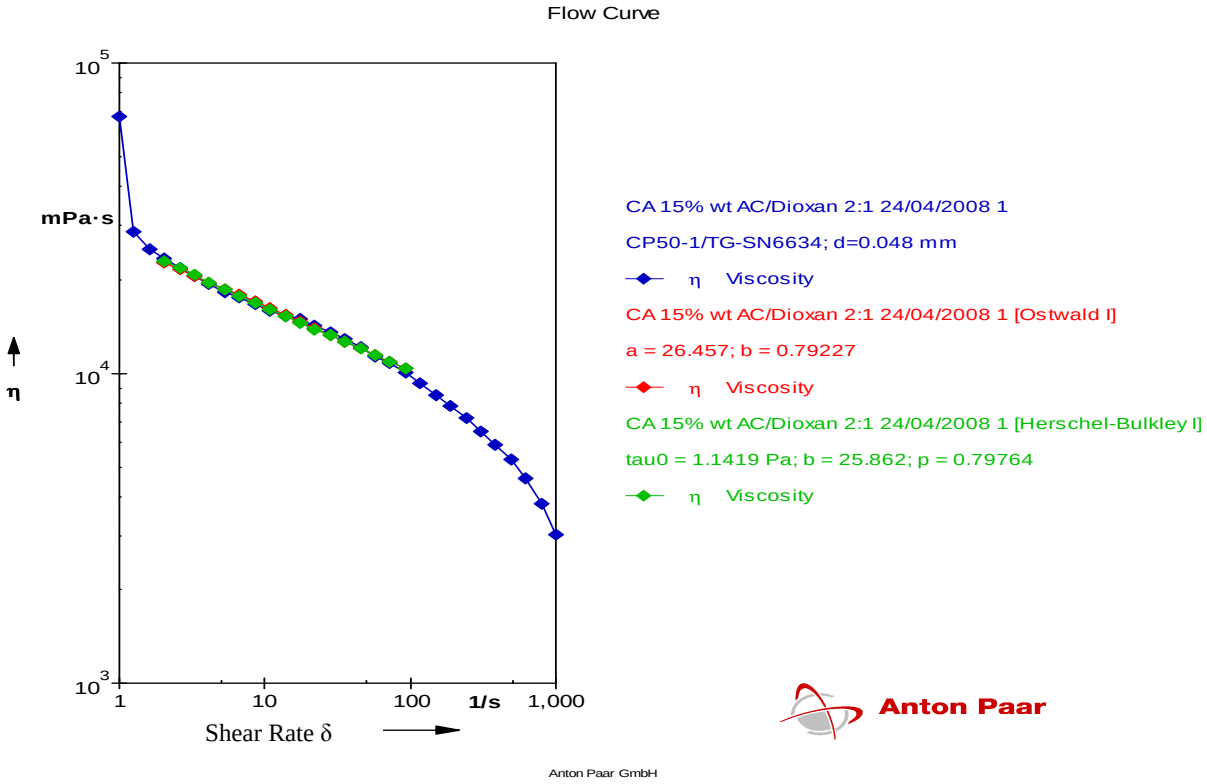
Flow Curve
10^5
mPa·s
η
10^4
10^3
1
10
100
1/s
1,000
Shear Rate δ
CA 15% wt AC/Dioxan 2:1 24/04/2008 1
CP50-1/TG-SN6634; d=0.048 mm
η Viscosity
CA 15% wt AC/Dioxan 2:1 24/04/2008 1 [Ostwald I]
a = 26.457; b = 0.79227
η Viscosity
CA 15% wt AC/Dioxan 2:1 24/04/2008 1 [Herschel-Bulkley I]
tau0 = 1.1419 Pa; b = 25.862; p = 0.79764
η Viscosity
Anton Paar
Anton Paar GmbH

Table B2: Values of viscosity and shear rate of CA (11, 12, 14 and 15 wt%)

Data Series Information

Name:	CA 11% wt AC/Dioxane 2:1 28/05/2008 2 [Herschel-Bulkley I]
Operator:	H Botha
Remarks:	Abdu Khalaf
Number of Intervals:	1
Application:	RHEOPLUS/32 V2.81 21002612-33025
Analysis Method:	Herschel-Bulkley I
Analysis Result:	tau0 = 4.7598 Pa; b = 1.6685; p = 0.87064

Meas. Pts.	Temperature [℃]	Shear Rate [1/s]	Shear Stress [Pa]	Viscosity [Pa·s]
1	******	2.04	7.87	3.85
2	******	2.59	8.58	3.31
3	******	3.29	9.47	2.88
4	******	4.18	10.6	2.53
5	******	5.3	11.9	2.24
6	******	6.72	13.5	2.01
7	******	8.53	15.5	1.82
8	******	10.8	18	1.67
9	******	13.7	21.1	1.54
10	******	17.4	24.9	1.43
11	******	22.1	29.5	1.33
12	******	28.1	35.2	1.25
13	******	35.6	42.2	1.18
14	******	45.2	50.8	1.12
15	******	57.4	61.5	1.07
16	******	72.8	74.5	1.02
17	******	92.4	90.6	0.981

Data Series Information

Name:	CA 12% wt AC/Dioxane 2:1 10/04/2008 2 [Herschel-Bulkley I]
Operator:	H Botha
Remarks:	Abdu Khalaf
Number of Intervals:	1
Application:	RHEOPLUS/32 V2.81 21002612-33025
Analysis Method:	Herschel-Bulkley I
Analysis Result:	tau0 = 10.261 Pa; b = 5.1204; p = 0.90801

Meas. Pts.	Temperature [℃]	Shear Rate [1/s]	Shear Stress [Pa]	Viscosity [Pa·s]
1	******	2.04	20.1	9.82
2	******	2.59	22.4	8.65
3	******	3.29	25.4	7.71
4	******	4.18	29	6.95
5	******	5.3	33.5	6.33
6	******	6.72	39.2	5.82
7	******	8.53	46.1	5.41
8	******	10.8	54.8	5.06
9	******	13.7	65.6	4.77
10	******	17.4	78.9	4.53

11	******	22.1	95.4	4.32
12	******	28.1	116	4.13
13	******	35.6	142	3.97
14	******	45.2	173	3.83
15	******	57.4	213	3.71
16	******	72.8	261	3.59
17	******	92.4	322	3.49

Data Series Information

Name:	CA 14% wt AC/Dioxane 2:1 10/04/2008 1 [Herschel-Bulkley I]
Operator:	H Botha
Remarks:	Abdu Khalaf
Number of Intervals:	1
Application:	RHEOPLUS/32 V2.81 21002612-33025
Analysis Method:	Herschel-Bulkley I
Analysis Result:	tau0 = 6.9255 Pa; b = 21.131; p = 0.84569

Meas. Pts.	Temperature [℃]	Shear Rate [1/s]	Shear Stress [Pa]	Viscosity [Pa·s]
1	******	2.04	45.6	22.3
2	******	2.59	54.2	20.9
3	******	3.29	64.8	19.7
4	******	4.18	77.7	18.6
5	******	5.3	93.5	17.6
6	******	6.72	113	16.8
7	******	8.53	136	16
8	******	10.8	165	15.3
9	******	13.7	201	14.6
10	******	17.4	244	14
11	******	22.1	297	13.4
12	******	28.1	362	12.9
13	******	35.6	441	12.4
14	******	45.2	537	11.9
15	******	57.4	656	11.4
16	******	72.8	801	11
17	******	92.4	978	10.6

Data Series Information

Name:	CA 11% wt AC/Dioxane 2:1 28/05/2008 2 [Ostwald I]
Operator:	H Botha
Remarks:	Abdu Khalaf
Number of Intervals:	1
Application:	RHEOPLUS/32 V2.81 21002612-33025
Analysis Method:	Ostwald I
Analysis Result:	a = 4.1867; b = 0.6516

Meas. Pts.	Temperature [℃]	Shear Rate [1/s]	Shear Stress [Pa]	Viscosity [Pa·s]
1	******	2.04	6.67	3.26
2	******	2.59	7.79	3
3	******	3.29	9.1	2.76
4	******	4.18	10.6	2.54
5	******	5.3	12.4	2.34

6	******	6.72	14.5	2.16
7	******	8.53	16.9	1.98
8	******	10.8	19.8	1.83
9	******	13.7	23.1	1.68
10	******	17.4	27	1.55
11	******	22.1	31.5	1.42
12	******	28.1	36.8	1.31
13	******	35.6	43	1.21
14	******	45.2	50.2	1.11
15	******	57.4	58.6	1.02
16	******	72.8	68.4	0.94
17	******	92.4	79.9	0.865

Data Series Information

Name:	CA 12% wt AC/Dioxane 2:1 10/04/2008 2 [Ostwald l]
Operator:	H Botha
Remarks:	Abdu Khalaf
Number of Intervals:	1
Application:	RHEOPLUS/32 V2.81 21002612-33025
Analysis Method:	Ostwald l
Analysis Result:	a = 10.193; b = 0.73992

Meas. Pts.	Temperature [℃]	Shear Rate [1/s]	Shear Stress [Pa]	Viscosity [Pa·s]
1	******	2.04	17.3	8.47
2	******	2.59	20.6	7.96
3	******	3.29	24.6	7.48
4	******	4.18	29.3	7.03
5	******	5.3	35	6.61
6	******	6.72	41.8	6.21
7	******	8.53	49.8	5.84
8	******	10.8	59.4	5.49
9	******	13.7	70.8	5.16
10	******	17.4	84.5	4.85
11	******	22.1	101	4.56
12	******	28.1	120	4.28
13	******	35.6	143	4.02
14	******	45.2	171	3.78
15	******	57.4	204	3.56
16	******	72.8	243	3.34
17	******	92.4	290	3.14

Data Series Information

Name:	CA 14% wt AC/Dioxane 2:1 10/04/2008 1 [Ostwald l]
Operator:	H Botha
Remarks:	Abdu Khalaf
Number of Intervals:	1
Application:	RHEOPLUS/32 V2.81 21002612-33025
Analysis Method:	Ostwald l
Analysis Result:	a = 24.592; b = 0.80851

Meas. Pts.	Temperature [℃]	Shear Rate [1/s]	Shear Stress [Pa]	Viscosity [Pa·s]
1	******	2.04	43.8	21.4

2	******	2.59	53.1	20.5
3	******	3.29	64.4	19.6
4	******	4.18	78.1	18.7
5	******	5.3	94.7	17.9
6	******	6.72	115	17.1
7	******	8.53	139	16.3
8	******	10.8	169	15.6
9	******	13.7	205	14.9
10	******	17.4	248	14.2
11	******	22.1	301	13.6
12	******	28.1	365	13
13	******	35.6	442	12.4
14	******	45.2	536	11.9
15	******	57.4	650	11.3
16	******	72.8	788	10.8
17	******	92.4	955	10.3

Data Series Information

Name:	CA 15% wt AC/Dioxane 2:1 24/04/2008 1 [Ostwald I]
Operator:	H Botha
Remarks:	Abdu Khalaf
Number of Intervals:	1
Application:	RHEOPLUS/32 V2.81 21002612-33025
Analysis Method:	Ostwald I
Analysis Result:	a = 26.457; b = 0.79227

Meas. Pts.	Temperature [℃]	Shear Rate [1/s]	Shear Stress [Pa]	Viscosity [Pa·s]
1	******	2.04	46.6	22.8
2	******	2.59	56.3	21.7
3	******	3.29	68	20.7
4	******	4.18	82.1	19.7
5	******	5.3	99.1	18.7
6	******	6.72	120	17.8
7	******	8.53	145	16.9
8	******	10.8	175	16.1
9	******	13.7	211	15.4
10	******	17.4	255	14.6
11	******	22.1	308	13.9
12	******	28.1	371	13.2
13	******	35.6	449	12.6
14	******	45.2	542	12
15	******	57.4	654	11.4
16	******	72.8	790	10.9
17	******	92.3	954	10.3

Data Series Information

Name:	CA 15 wt% AC/Dioxane 2:1 24/04/2008 1 [Herschel-Bulkley I]
Operator:	H Botha
Remarks:	Abdu Khalaf
Number of Intervals:	1
Application:	RHEOPLUS/32 Demo V2.66 DEMO-DEMO
Analysis Method:	Herschel-Bulkley I
Analysis Result:	tau0 = 1.1419 Pa; b = 25.862; p = 0.79764

Meas. Pts.	Temperature [℃]	Shear Rate [1/s]	Shear Stress [Pa]	Viscosity [Pa·s]
1	******	2.04	46.9	22.9
2	******	2.59	56.4	21.8
3	******	3.29	68	20.7
4	******	4.18	82	19.6
5	******	5.3	98.9	18.7
6	******	6.72	119	17.8
7	******	8.53	144	16.9
8	******	10.8	174	16.1
9	******	13.7	210	15.3
10	******	17.4	254	14.6
11	******	22.1	307	13.9
12	******	28.1	371	13.2
13	******	35.6	448	12.6
14	******	45.2	542	12
15	******	57.4	655	11.4
16	******	72.8	792	10.9
17	******	92.3	957	10.4

B.2 Ostwald's model

$\eta = a\,\delta^{b}$

$\mathrm{Ln}(\eta) = \ln(a) + b.\ln(\delta)$

$$b = \frac{Y_2 - Y_1}{X_2 - X_1}$$

where $Y = \eta$ and $X = \delta$

$K = \exp(a)$

where η is the shear viscosity of the fluid, δ is the shear rate, K (intercept) = exp (a), and b can be expressed as (n-1) where n is called the power-low index. For a shear thinning fluid n <1

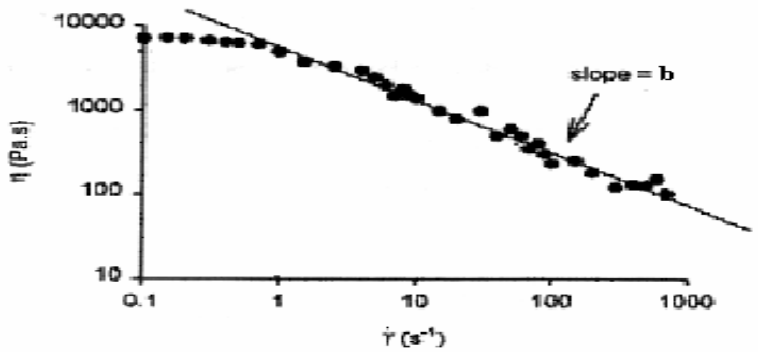

Figure B1: Typical behaviour for pseudoplastic fluid type [61]

C.1 The regression equation for the matrix i

Example $Y = b_0 + b_1x_1 + b_2x_2 + b_{12}x_1x_2 + b_3x_3 + b_{13}x_1x_3 + b_{23}x_2x_3 + b_{123}x_1x_2x_3$

where Y is the response (ID and OD), b_0 a constant, i.e., response at the zero level experiment, b1, b2, b3 and b4 are the linear coefficients (independent parameters), b12, b13, b14, b23, b24, b34, b123, b134, b234, b1234 are interaction coefficients representing the parameters in their coded form.

C.2 Diagnostics

In Figure C1, the points on this plot lie approximately on a straight line on the normal plot of residuals. Supporting that A, C, D, AC, AD, BD and ABD are the most significant effects. Figure C2 shows the plot of residuals versus predicted data points. The plot confirms that the residuals have a constant variance. The random scatter in the plot of residuals versus experimental run order in Figure C3 eliminates the possibility of a time related variable lurking in the background. The Box-Cox plot (Figure C4) recommends performing a log transformation.

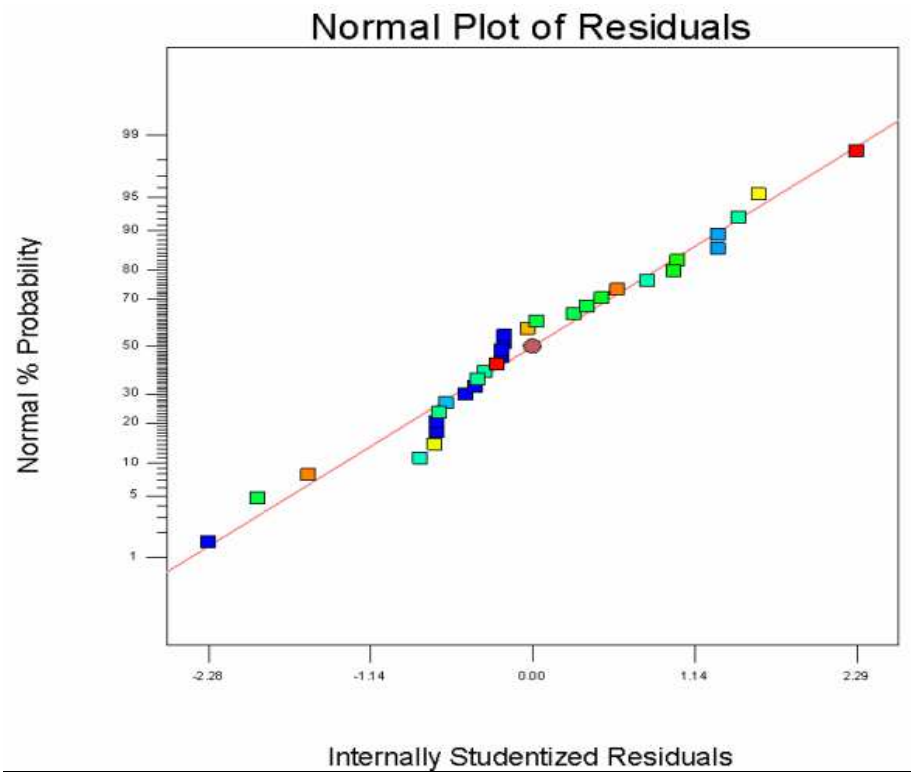

Figure C1: Normal plot of residuals (ID).

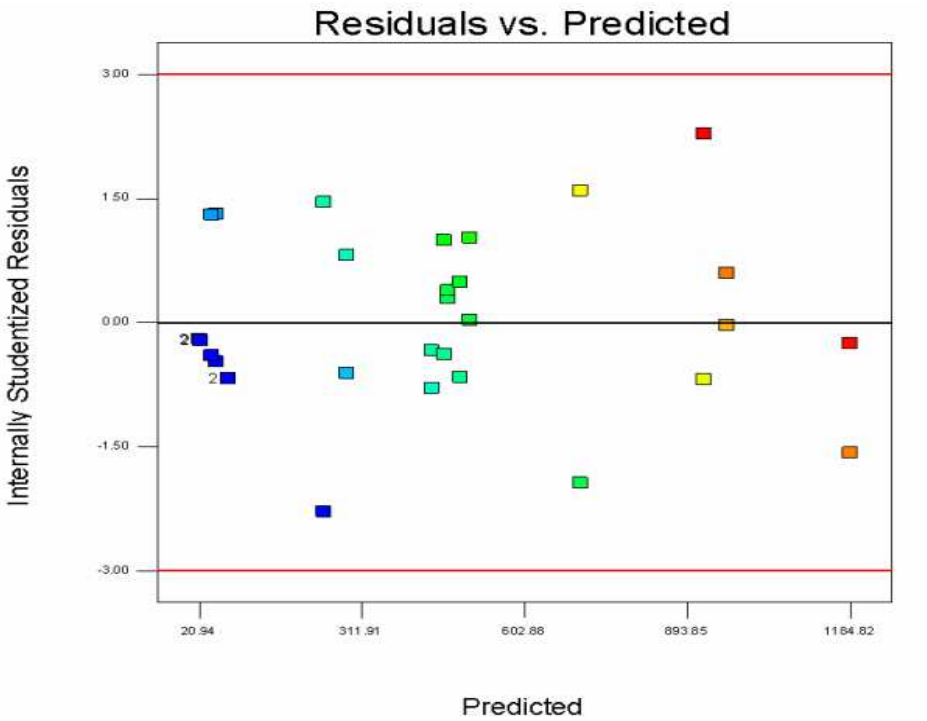

Figure C2: Plot of residuals vs. predicted data points (ID).

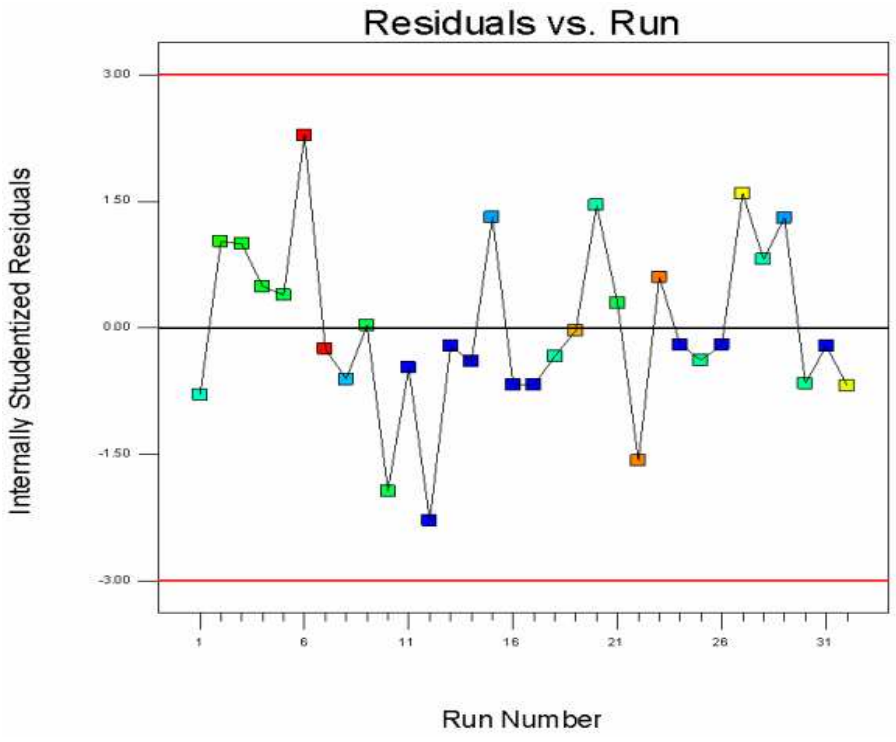

Figure C3: Plot of residuals vs. experimental run order (ID).

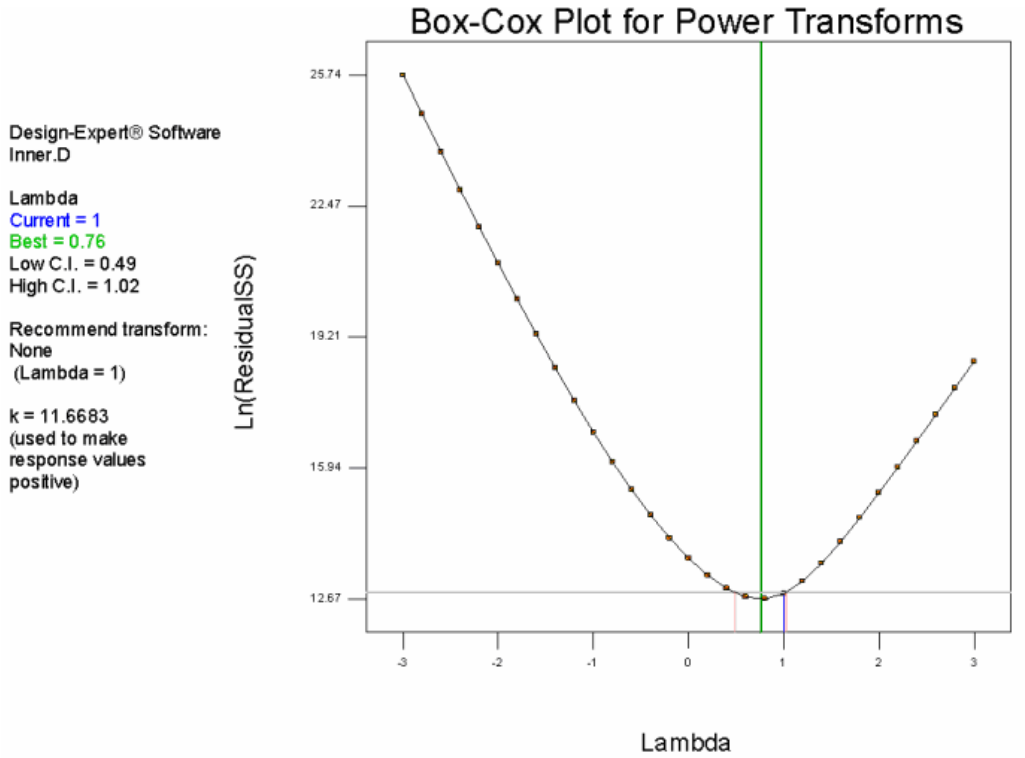

Figure C4: Box-Cox plot for power transforms (ID).

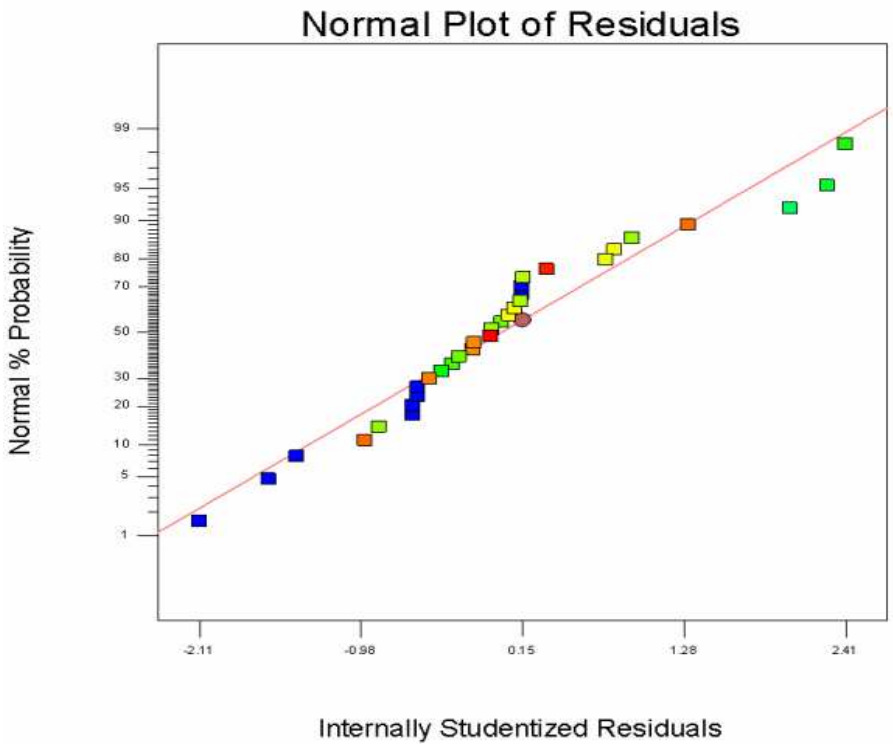

Figure C5: Normal plot of residuals (OD).

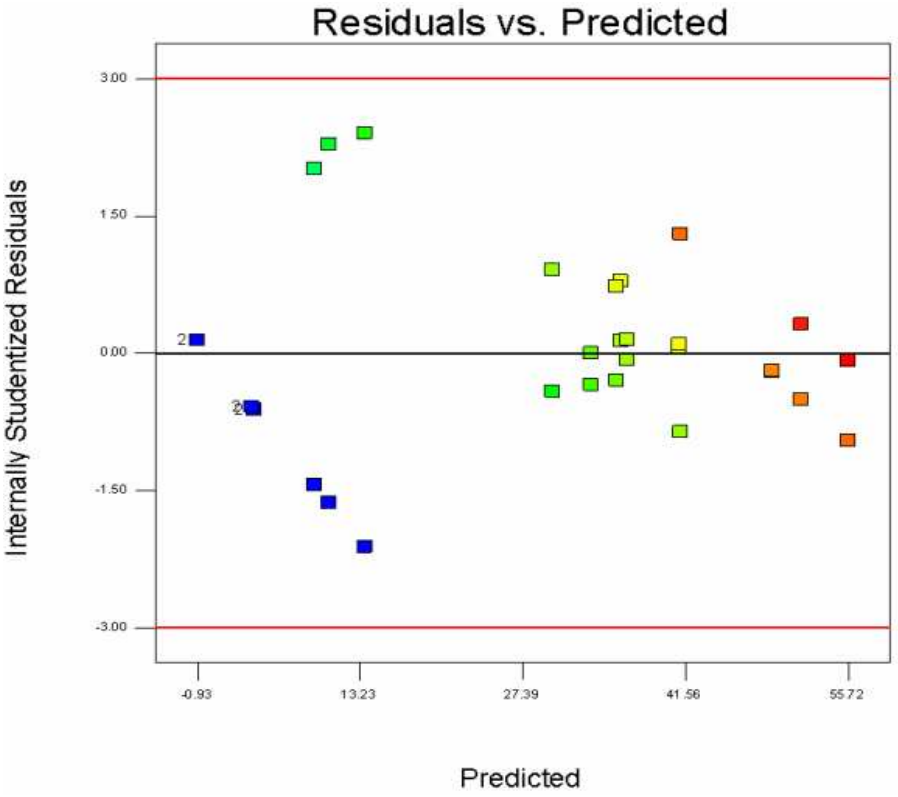

Figure C6: Plot of residuals vs. predicted data points (OD).

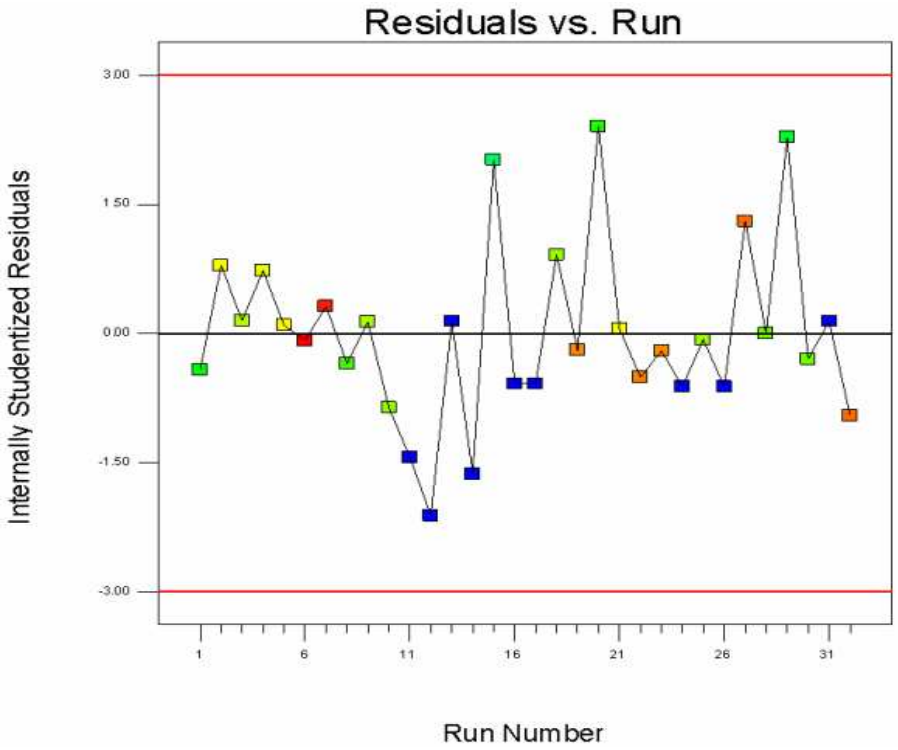

Figure C7: Plot of residuals vs. experimental run order (OD).

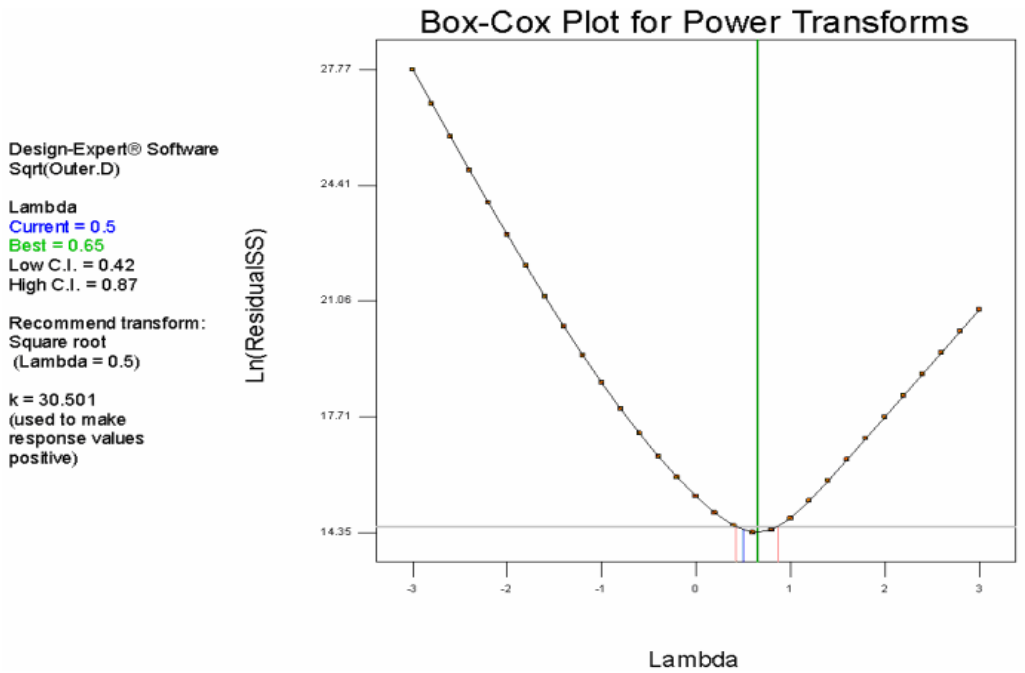

Figure C8: Box-Cox plot for power transforms (OD).

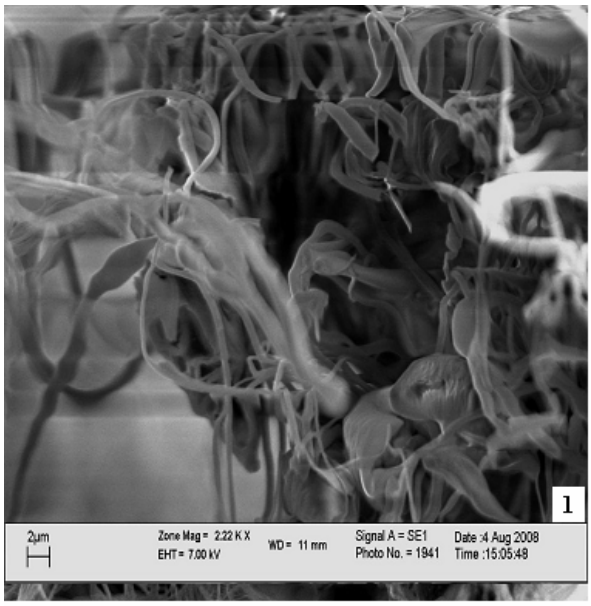
1
2μm
Zone Mag = 2.22 K X
EHT = 7.00 kV
WD = 11 mm
Signal A = SE1
Photo No. = 1941
Date :4 Aug 2008
Time :15:05:48

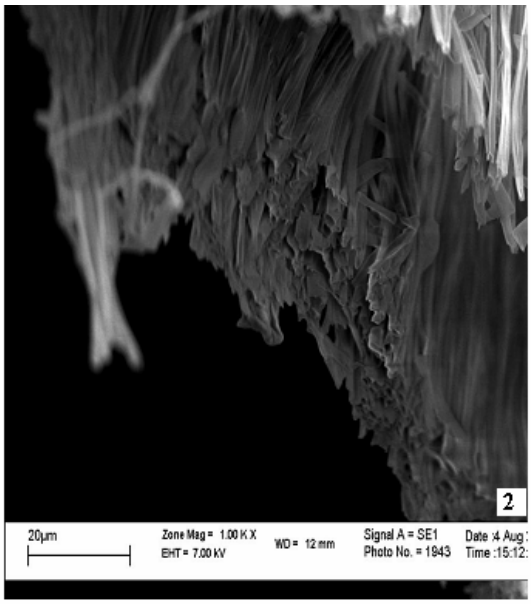
2
20μm
Zone Mag = 1.00 K X
EHT = 7.00 kV
WD = 12 mm
Signal A = SE1
Photo No. = 1943

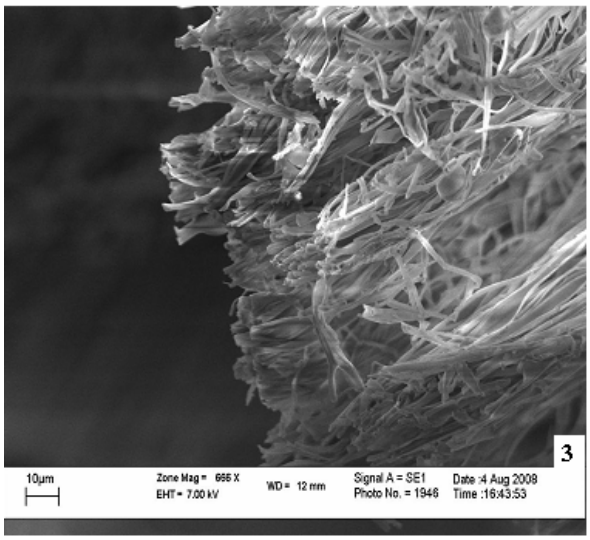
3
10μm
Zone Mag = 666 X
EHT = 7.00 kV
WD = 12 mm
Signal A = SE1
Photo No. = 1946
Date :4 Aug 2008
Time :16:43:53

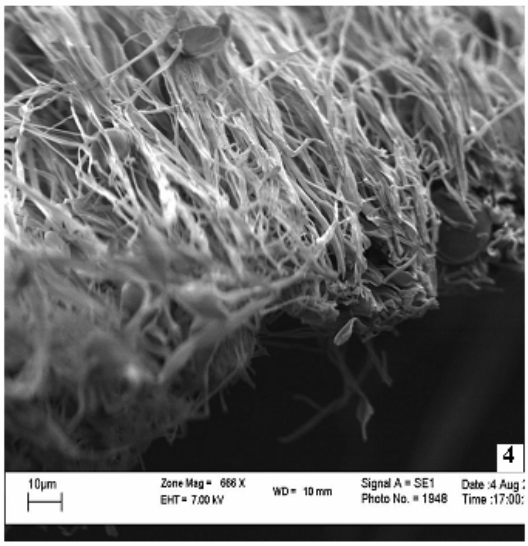
4
10μm
Zone Mag = 666 X
EHT = 7.00 kV
WD = 10 mm
Signal A = SE1
Photo No. = 1948

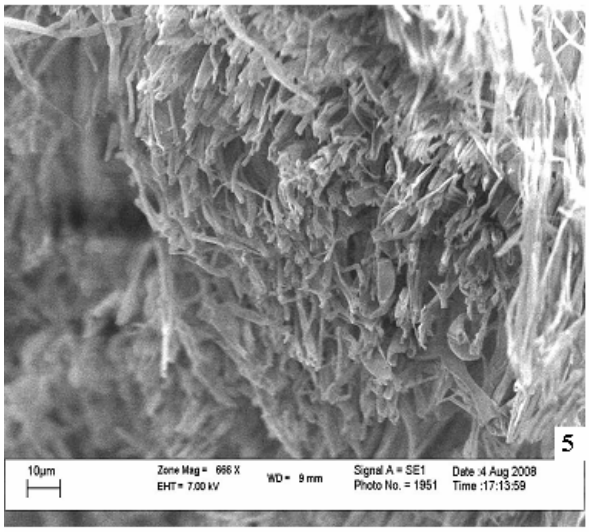
5
10μm
Zone Mag = 666 X
EHT = 7.00 kV
WD = 9 mm
Signal A = SE1
Photo No. = 1951
Date :4 Aug 2008
Time :17:13:59

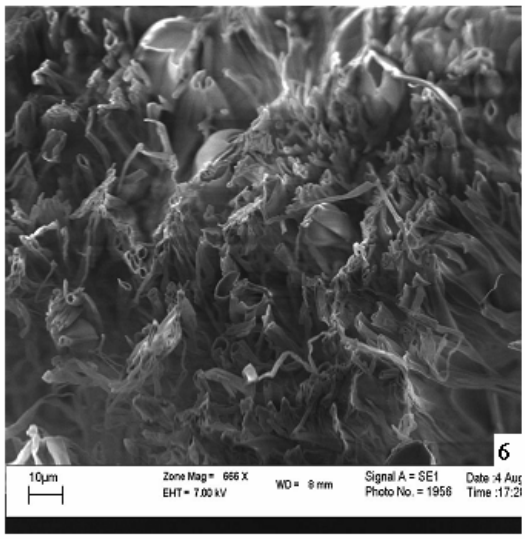
6
10μm
Zone Mag = 666 X
EHT = 7.00 kV
WD = 9 mm
Signal A = SE1
Photo No. = 1956

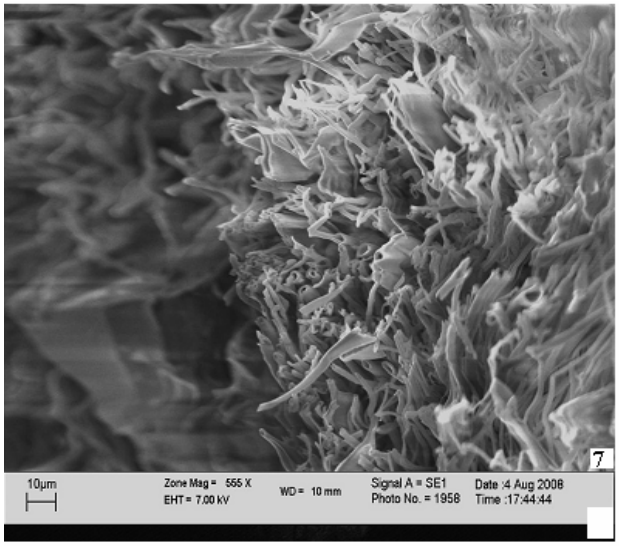
7
10µm
Zone Mag = 555 X
EHT = 7.00 kV
WD = 10 mm
Signal A = SE1
Photo No. = 1958
Date :4 Aug 2008
Time :17:44:44

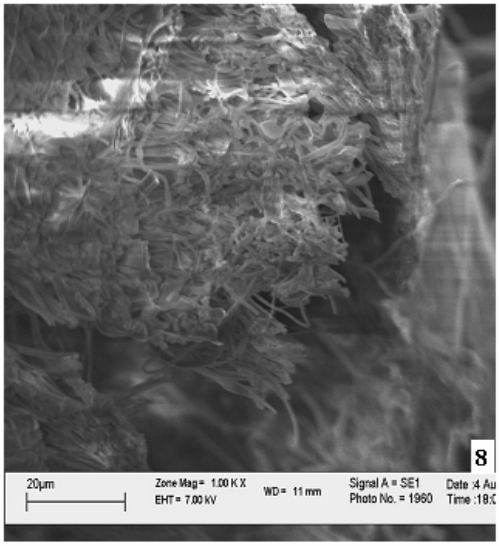
8
20µm
Zone Mag = 1.00 K X
EHT = 7.00 kV
WD = 11 mm
Signal A = SE1
Photo No. = 1960

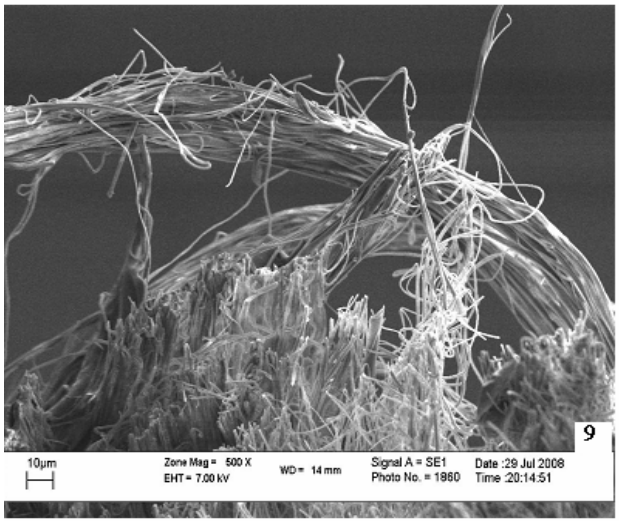
9
10µm
Zone Mag = 500 X
EHT = 7.00 kV
WD = 14 mm
Signal A = SE1
Photo No. = 1960
Date :29 Jul 2008
Time :20:14:51

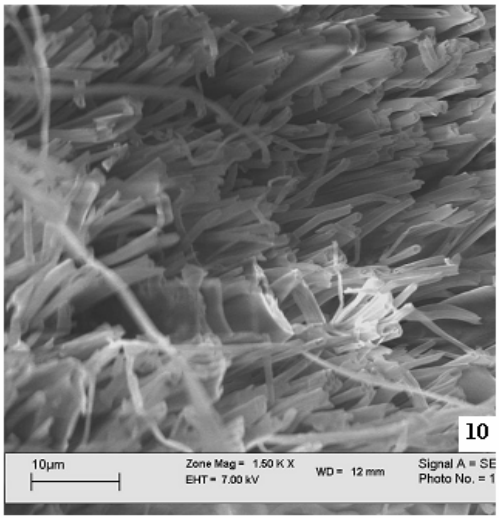
10
10µm
Zone Mag = 1.50 K X
EHT = 7.00 kV
WD = 12 mm

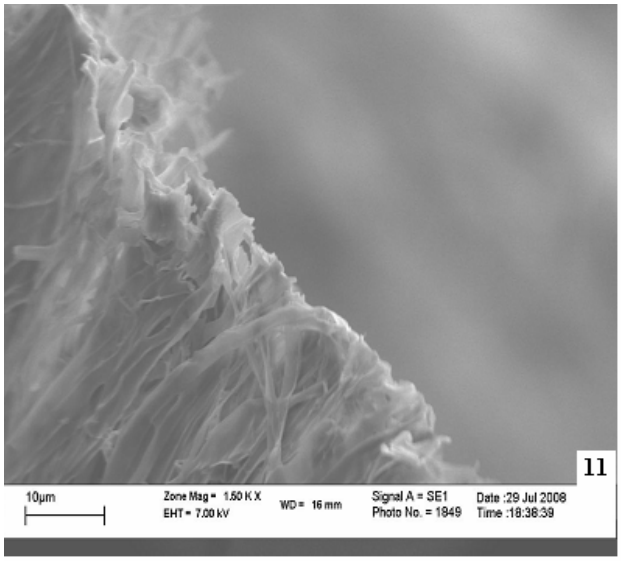
11
10µm
Zone Mag = 1.50 K X
EHT = 7.00 kV
WD = 16 mm
Signal A = SE1
Photo No. = 1849
Date :29 Jul 2008
Time :18:38:39

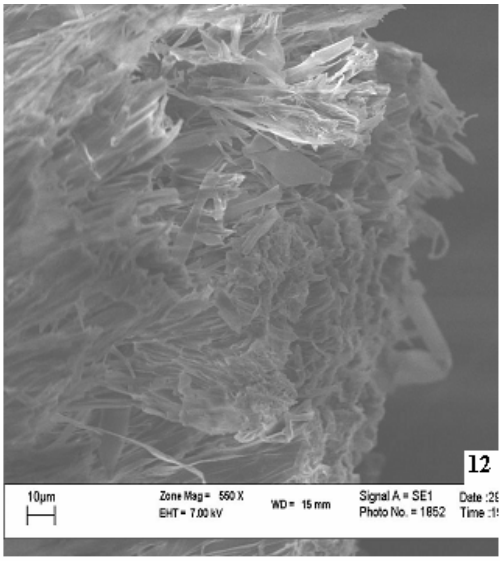
12
10µm
Zone Mag = 550 X
EHT = 7.00 kV
WD = 15 mm
Signal A = SE1
Photo No. = 1852

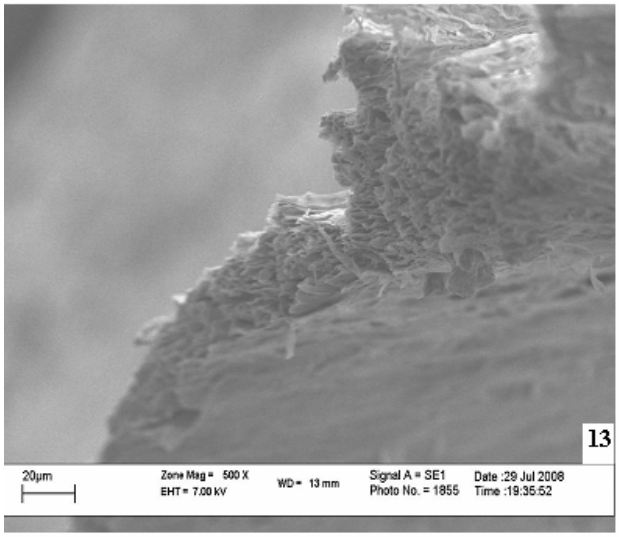
13
20µm
Zone Mag = 500 X
EHT = 7.00 kV
WD = 13 mm
Signal A = SE1
Photo No. = 1855
Date :29 Jul 2008
Time :19:35:52

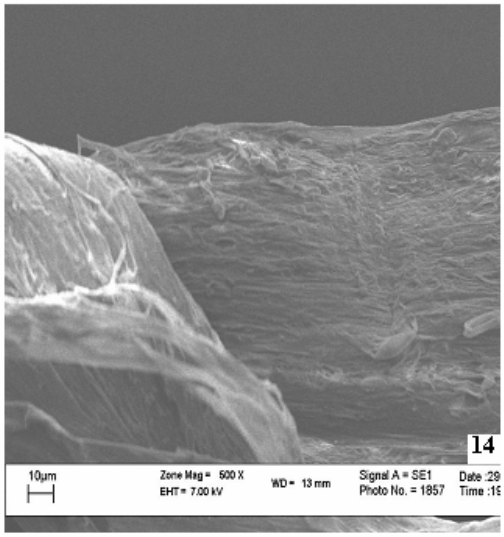
14
10µm
Zone Mag = 500 X
EHT = 7.00 kV
WD = 13 mm
Signal A = SE1
Photo No. = 1857

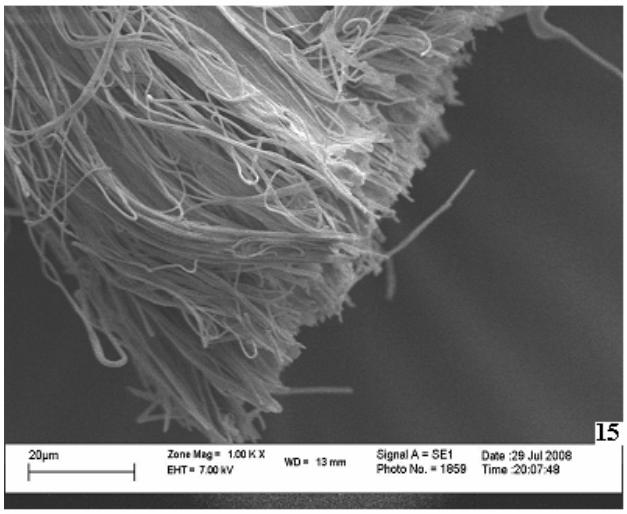
15
20µm
Zone Mag = 1.00 K X
EHT = 7.00 kV
WD = 13 mm
Signal A = SE1
Photo No. = 1859
Date :29 Jul 2008
Time :20:07:49

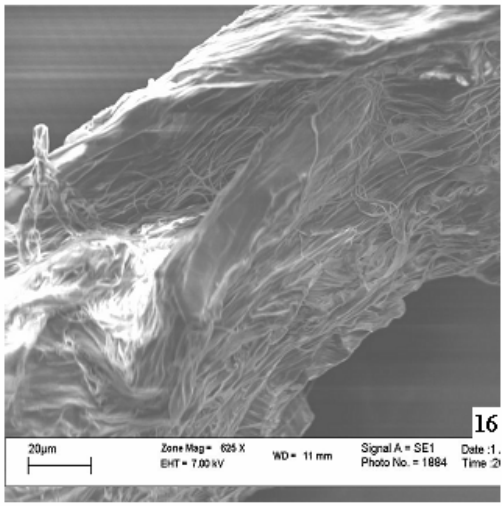
16
20µm
Zone Mag = 625 X
EHT = 7.00 kV
WD = 11 mm
Signal A = SE1
Photo No. = 1884

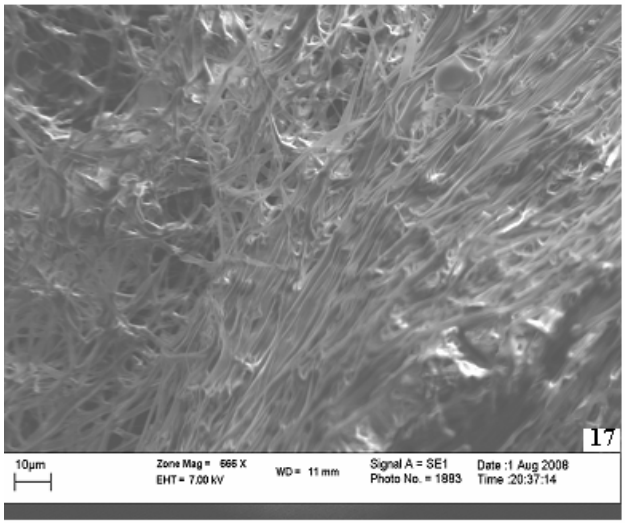
17
10µm
Zone Mag = 666 X
EHT = 7.00 kV
WD = 11 mm
Signal A = SE1
Photo No. = 1883
Date :1 Aug 2008
Time :20:37:14

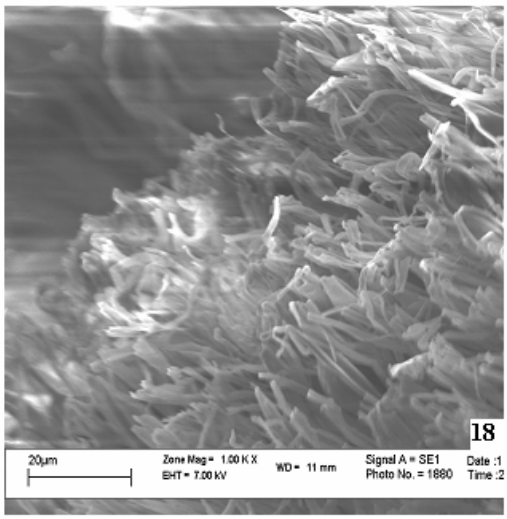
18
20µm
Zone Mag = 1.00 K X
EHT = 7.00 kV
WD = 11 mm
Signal A = SE1
Photo No. = 1880

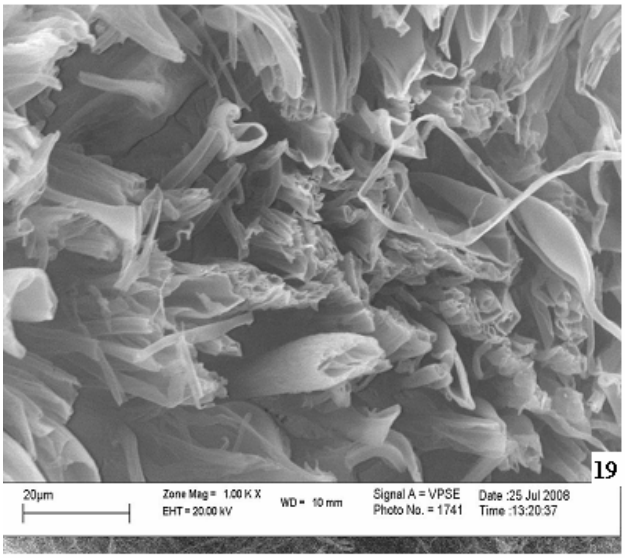
19
20µm
Zone Mag = 1.00 K X
EHT = 20.00 kV
WD = 10 mm
Signal A = VPSE
Photo No. = 1741
Date :25 Jul 2008
Time :13:20:37

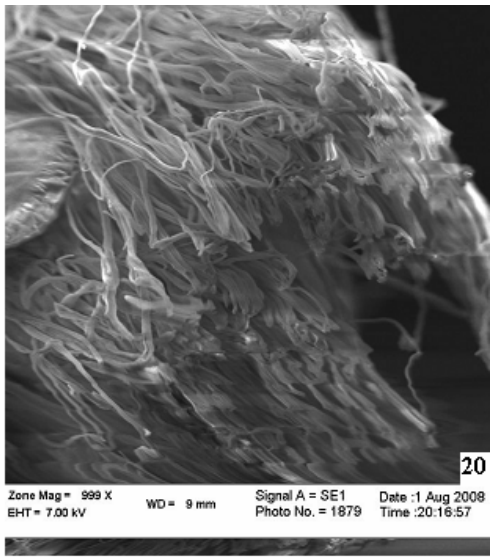
20
Zone Mag = 999 X
EHT = 7.00 kV
WD = 9 mm
Signal A = SE1
Photo No. = 1879
Date :1 Aug 2008
Time :20:16:57

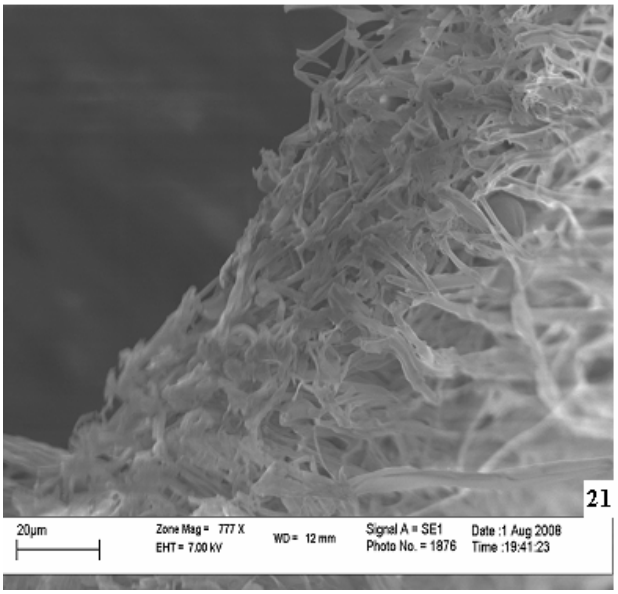
21
20µm
Zone Mag = 777 X
EHT = 7.00 kV
WD = 12 mm
Signal A = SE1
Photo No. = 1876
Date :1 Aug 2008
Time :19:41:23

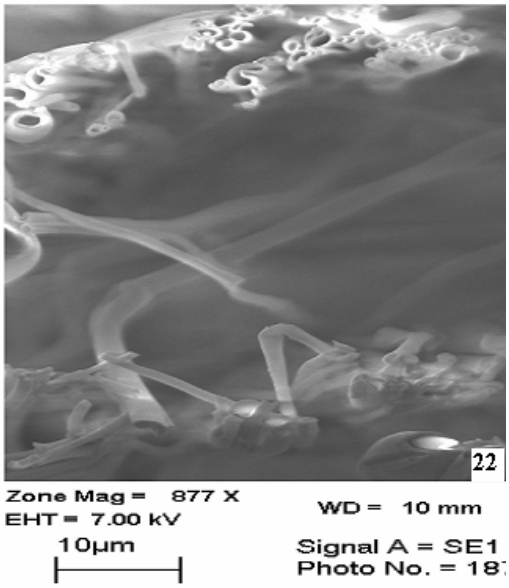
22
Zone Mag = 877 X
EHT = 7.00 kV
10µm
WD = 10 mm
Signal A = SE1
Photo No. = 187

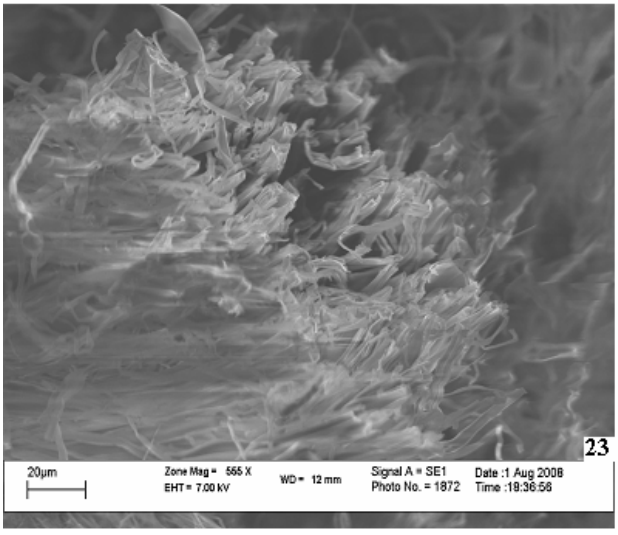
23
20µm
Zone Mag = 555 X
EHT = 7.00 kV
WD = 12 mm
Signal A = SE1
Photo No. = 1872
Date :1 Aug 2008
Time :19:36:56

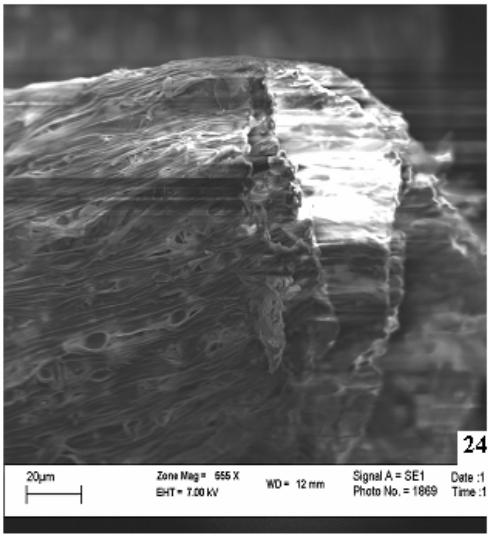
24
20µm
Zone Mag = 555 X
EHT = 7.00 kV
WD = 12 mm
Signal A = SE1
Photo No. = 1869
Date :1
Time :1

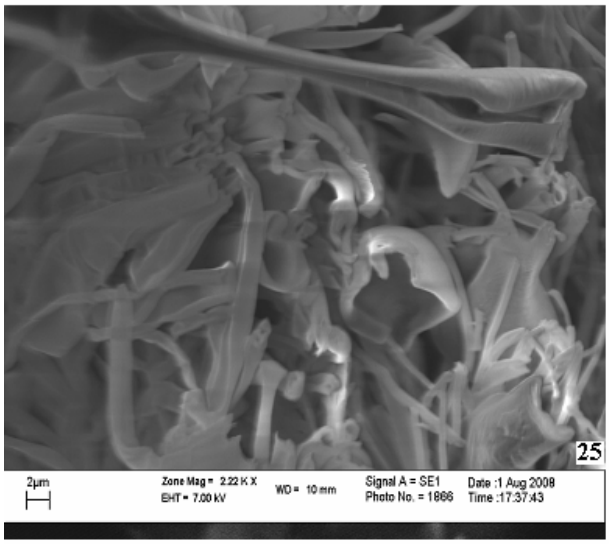
25
2µm
Zone Mag = 2.22 K X
EHT = 7.00 kV
WD = 10 mm
Signal A = SE1
Photo No. = 1866
Date :1 Aug 2008
Time :17:37:43

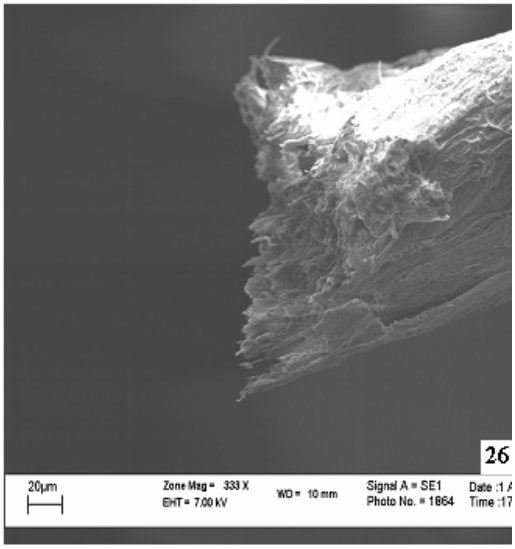
26
20µm
Zone Mag = 333 X
EHT = 7.00 kV
WD = 10 mm
Signal A = SE1
Photo No. = 1864

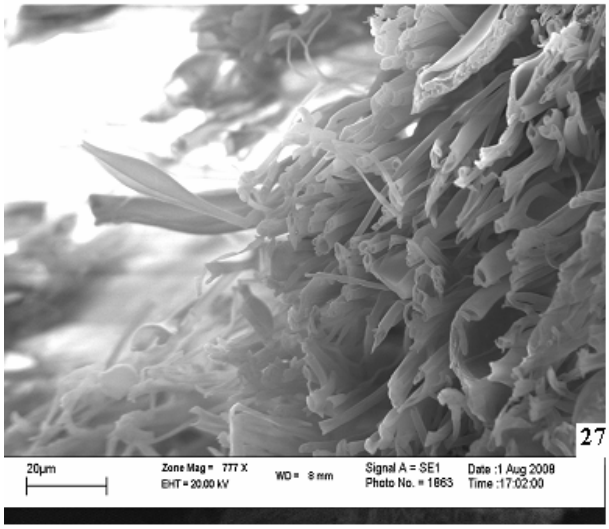
27
20µm
Zone Mag = 777 X
EHT = 20.00 kV
WD = 8 mm
Signal A = SE1
Photo No. = 1863
Date :1 Aug 2008
Time :17:02:00

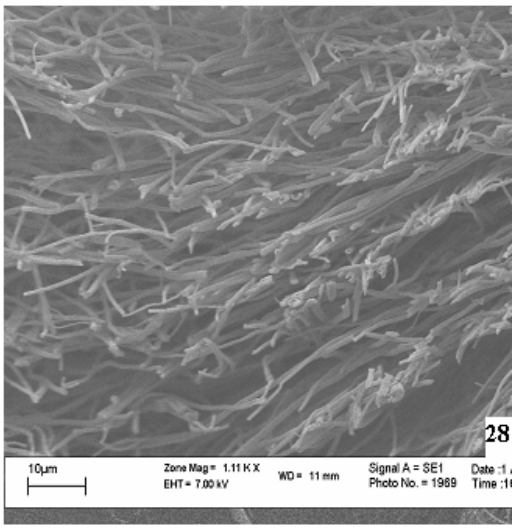
28
10µm
Zone Mag = 1.11 K X
EHT = 7.00 kV
WD = 11 mm
Signal A = SE1
Photo No. = 1969

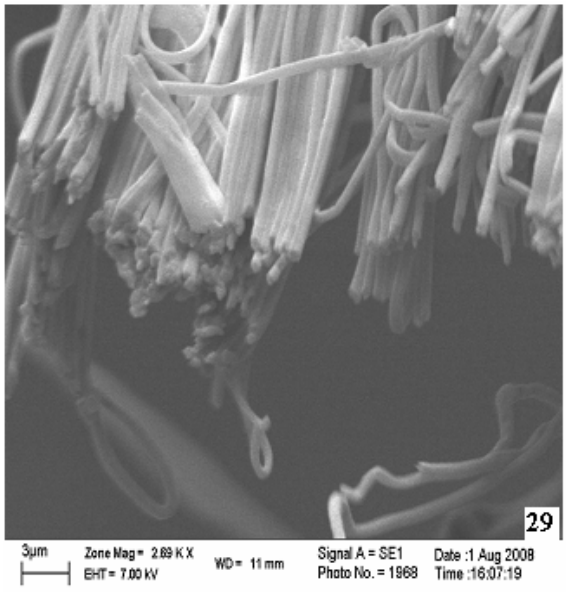
29
3µm
Zone Mag = 2.69 K X
EHT = 7.00 kV
WD = 11 mm
Signal A = SE1
Photo No. = 1968
Date :1 Aug 2008
Time :16:07:19

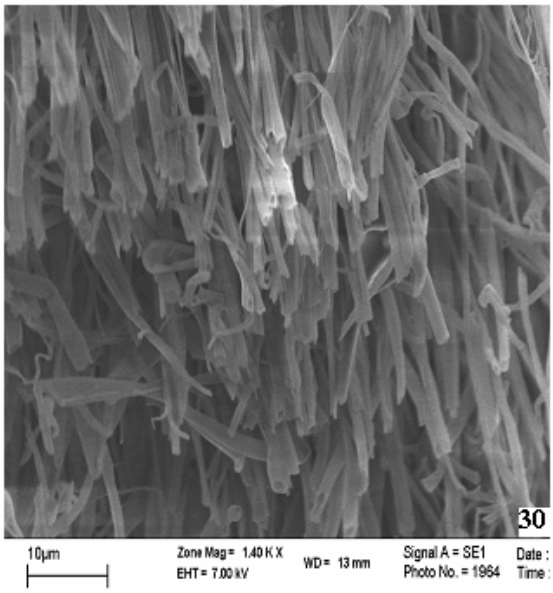
30
10µm
Zone Mag = 1.40 K X
EHT = 7.00 kV
WD = 13 mm
Signal A = SE1
Photo No. = 1964

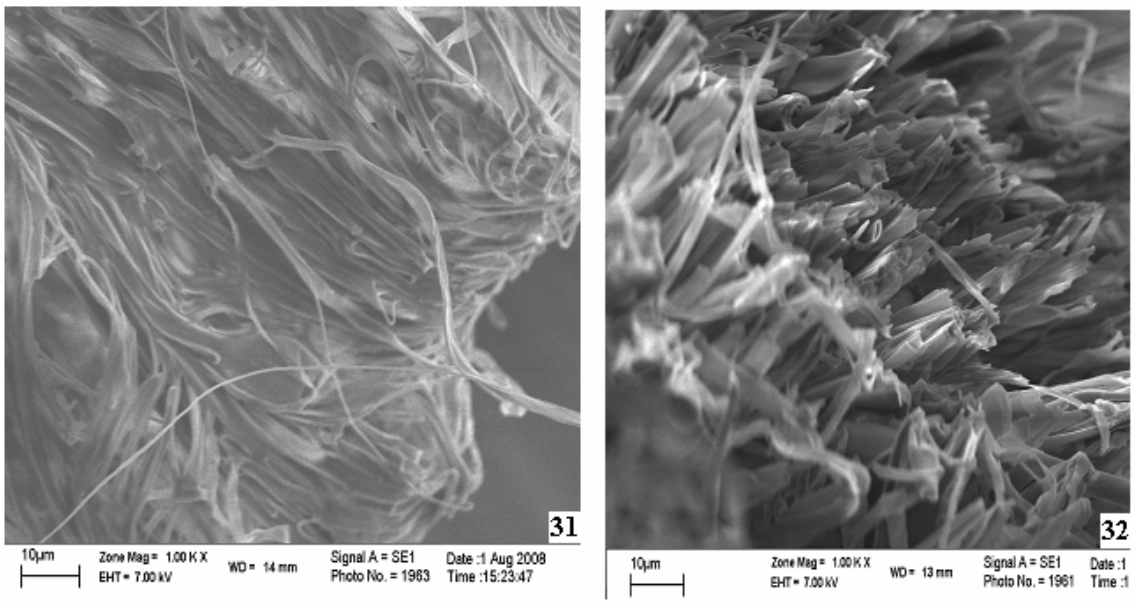

Figure D1: (1-32) SEM images obtained for samples from all 32 runs of factorial designs of experiments.

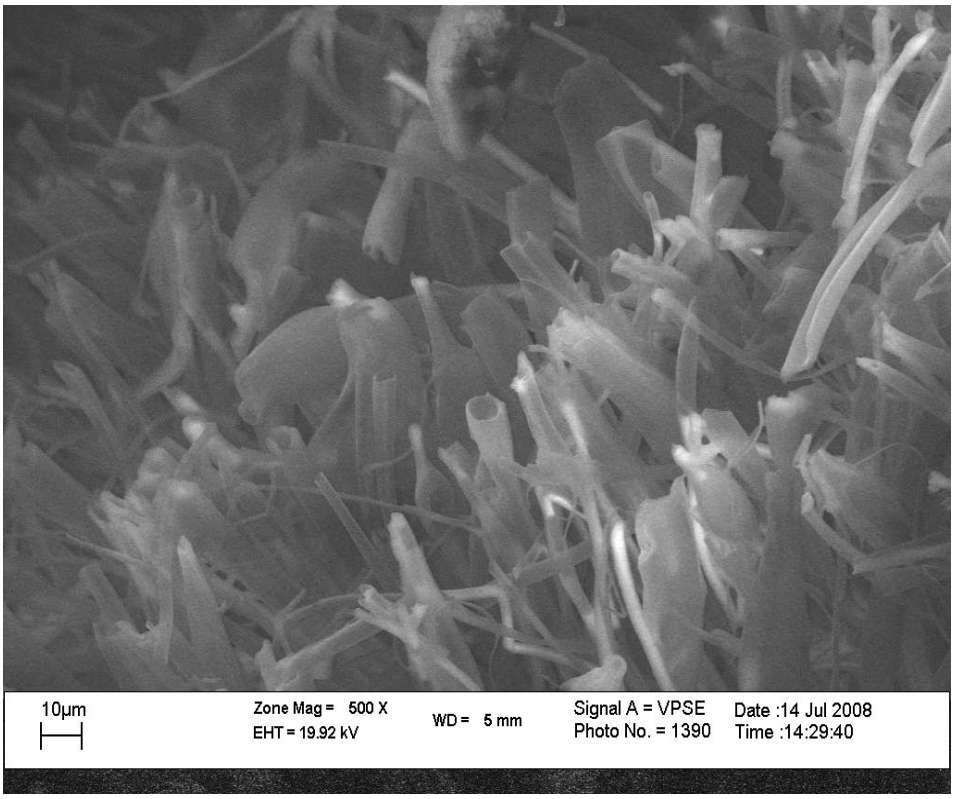

Figure D2: SEM image of electrospun 14 wt % CA hollow fibers.

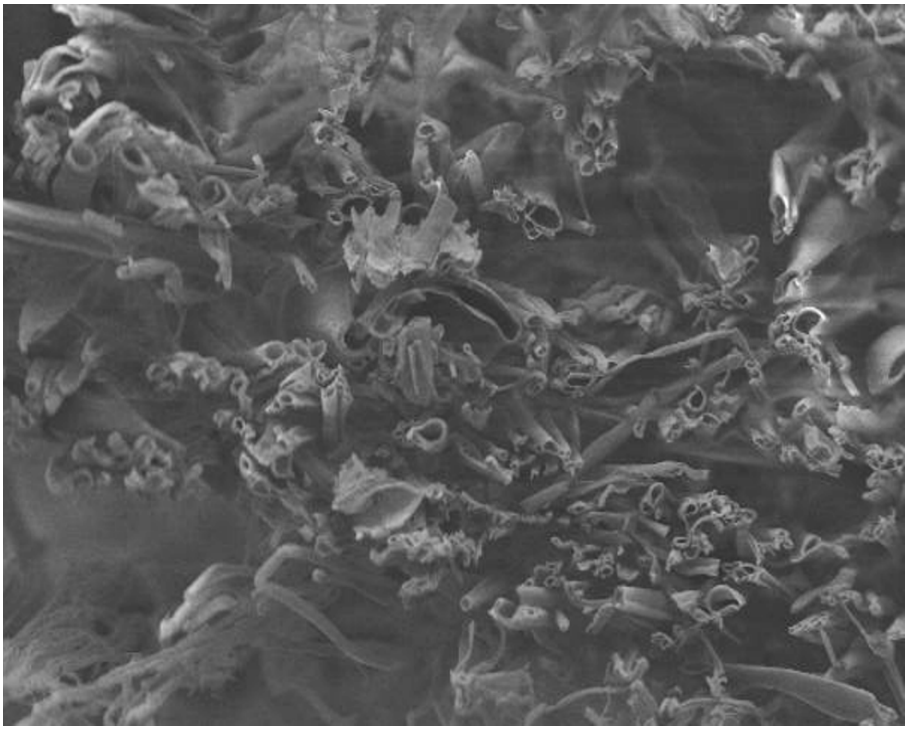

(A)

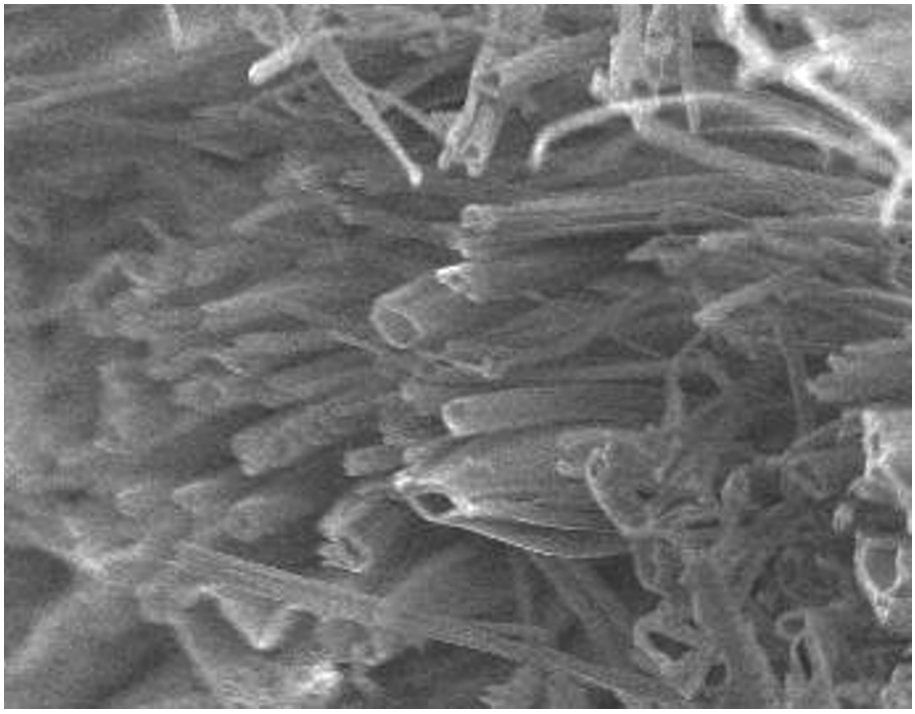

(B)

Figure D3: SEM images of electrospun of 14 wt % hollow fibers. (A) Mag (444 x). (B) Magnification (444x).

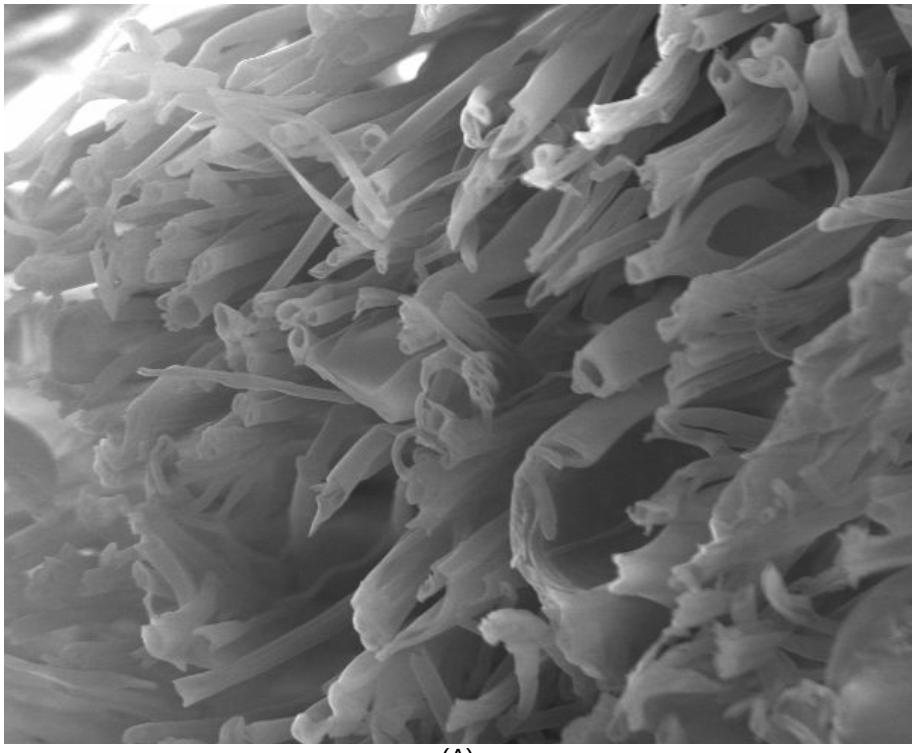

(A)

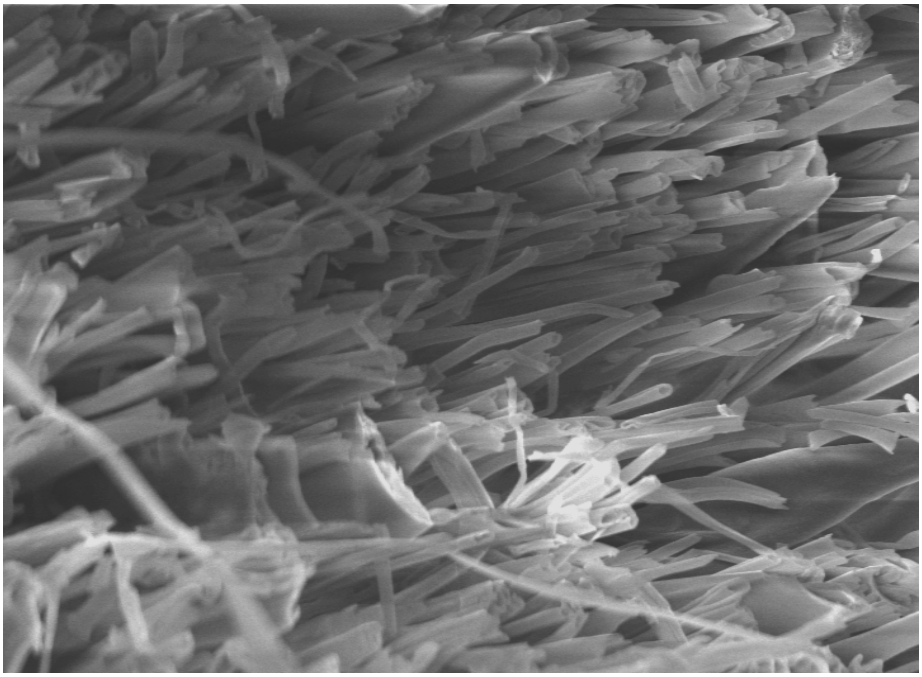

(B)

Figure D4: SEM image of hollow CA fibers prepared by the coaxial electrospinning technique: (a) 872 nm (core) and 2458 (shell), Mag (777), b) 495 nm (core) and 1266 nm (shell), Mag (1500).

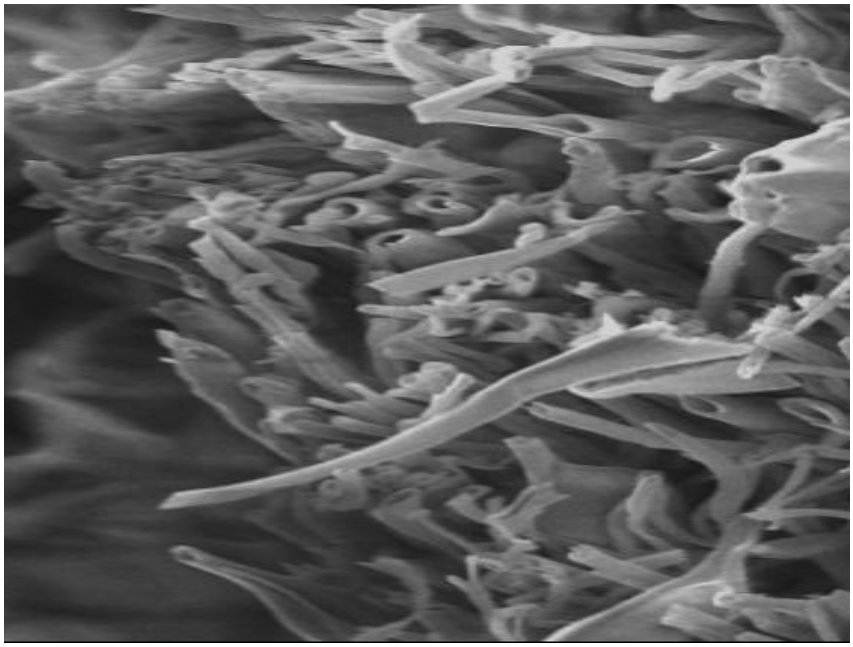

Figure D5: SEM image of electrospun hollow CA fibers produced using a CA polymer concentration of 14 wt % at a distance of 11 cm, Mag (555x).

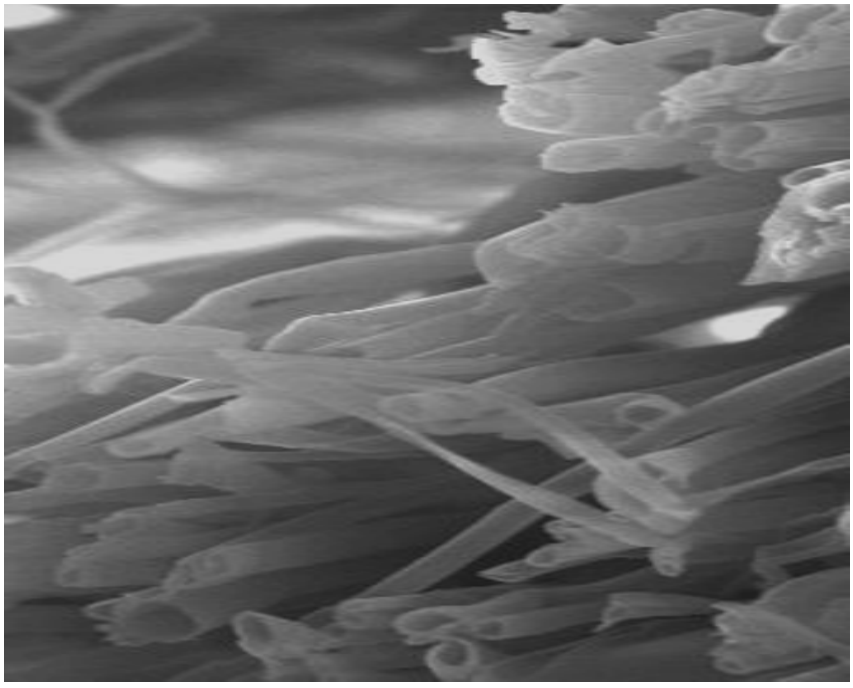

Figure D6: SEM image of electrospun hollow CA fibers produced using a CA polymer concentration of 14 wt % at a distance of 8 cm, Mag (777x).

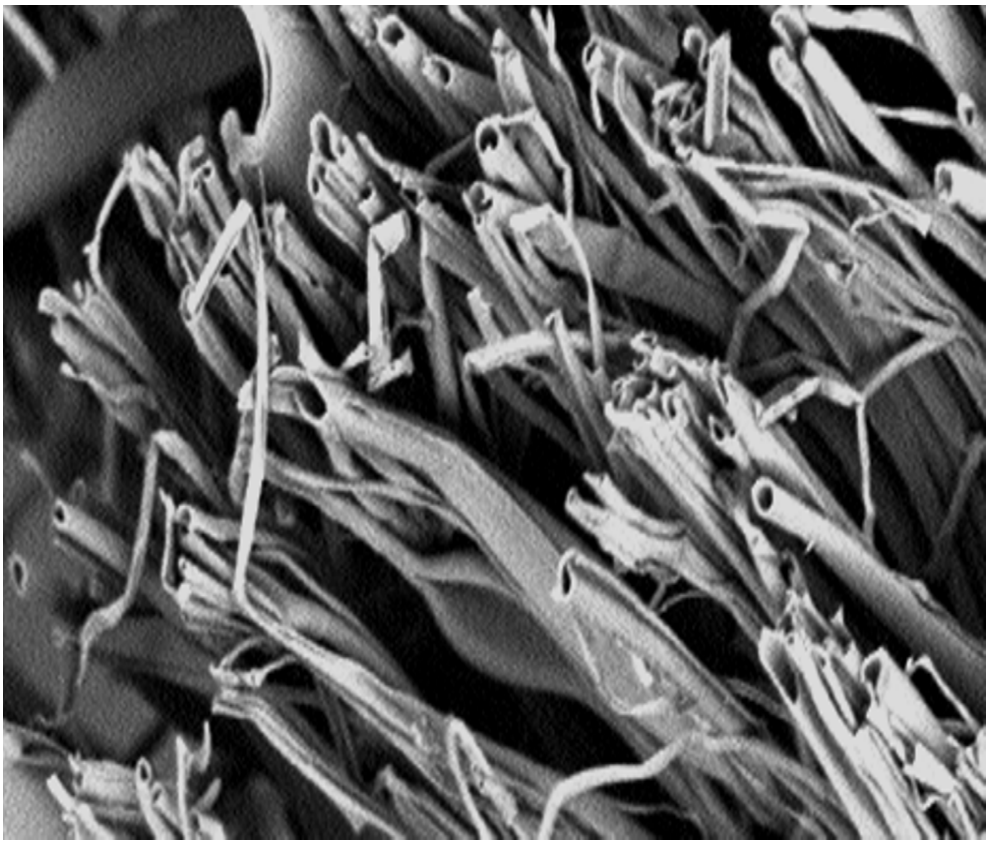

Figure D7: SEM image of electrospun hollow fibers produced using a CA of 14 wt % and 1m/hr and 3 ml/hr core and shell feed rates, respectively, Mag (1200x).

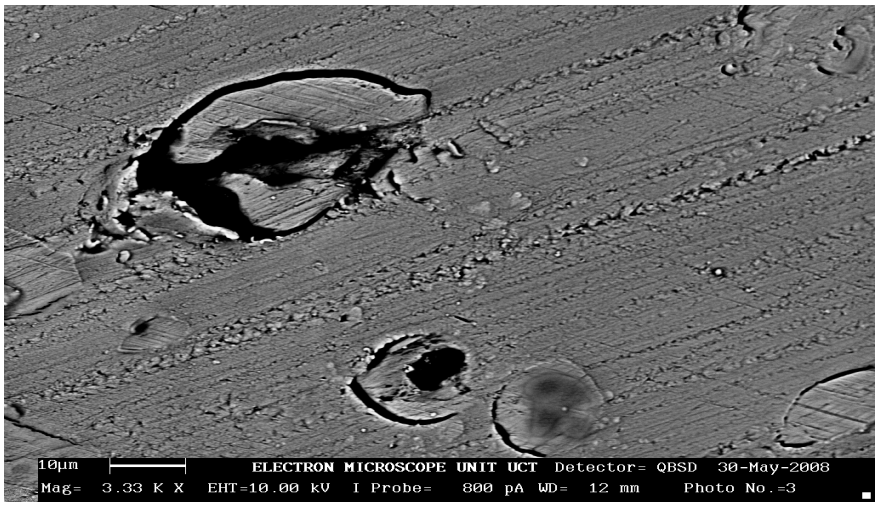

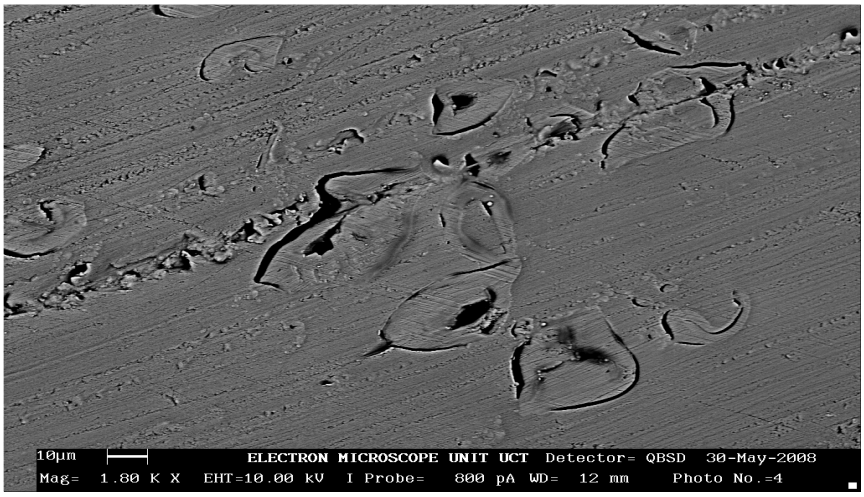

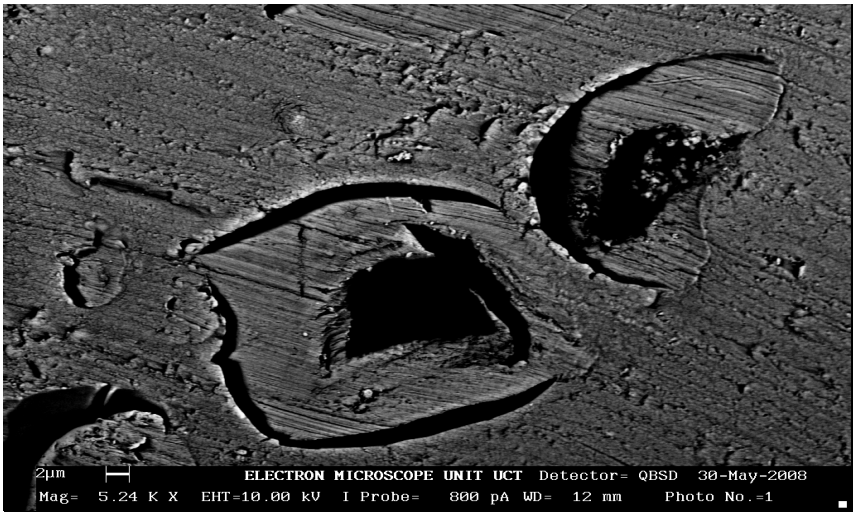

Figure D8: SEM images of serial sections of electrospun hollow CA fibers obtained using a microtome.

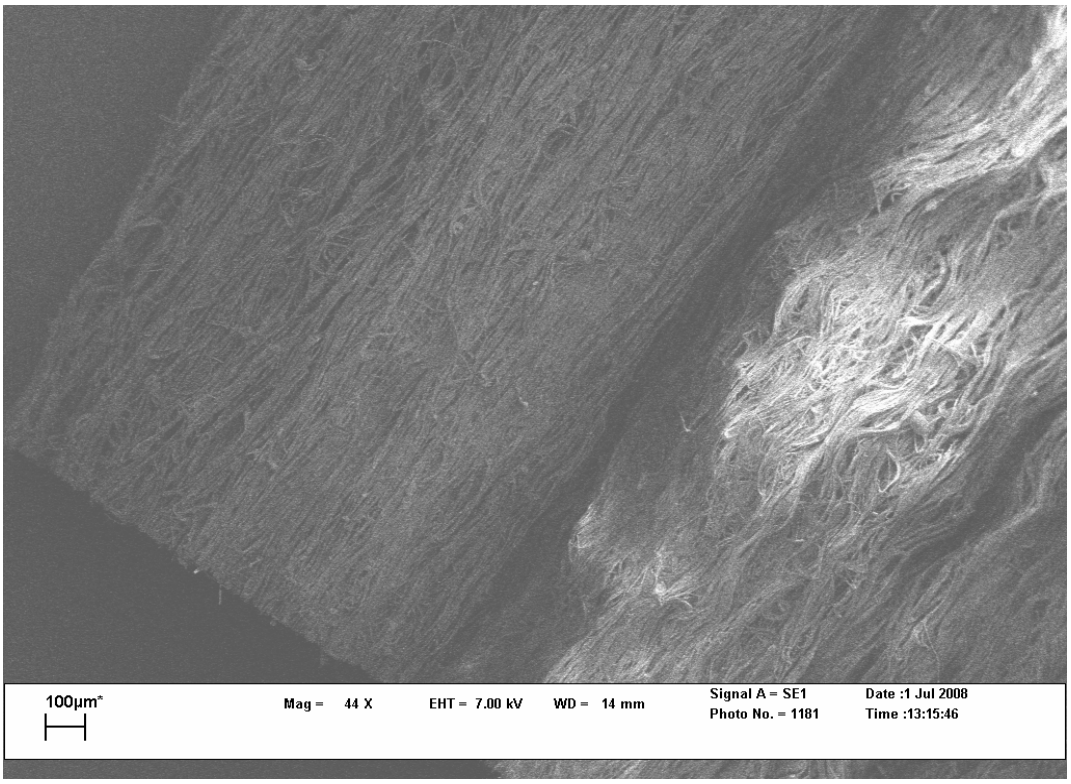

Figure D 9: SEM images of well alignment of CA fibers.

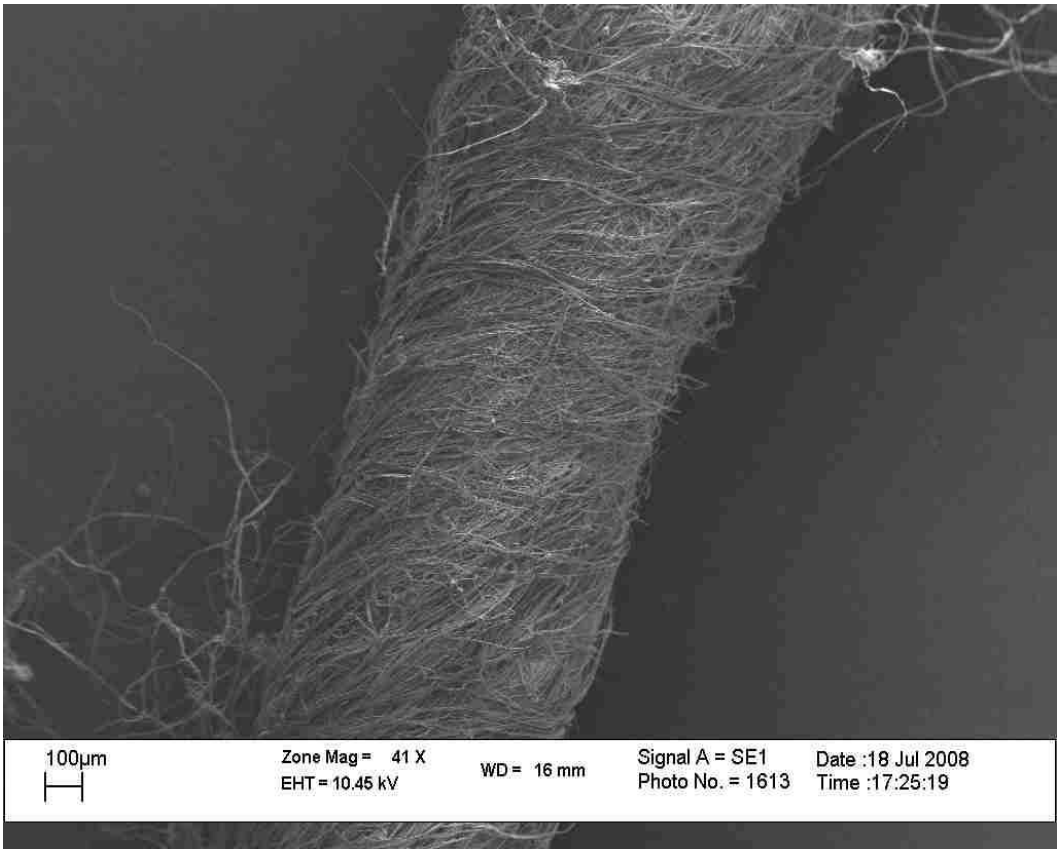

Figure D10: Electrospun fiber yarn of CA showing high degree of fiber alignment.

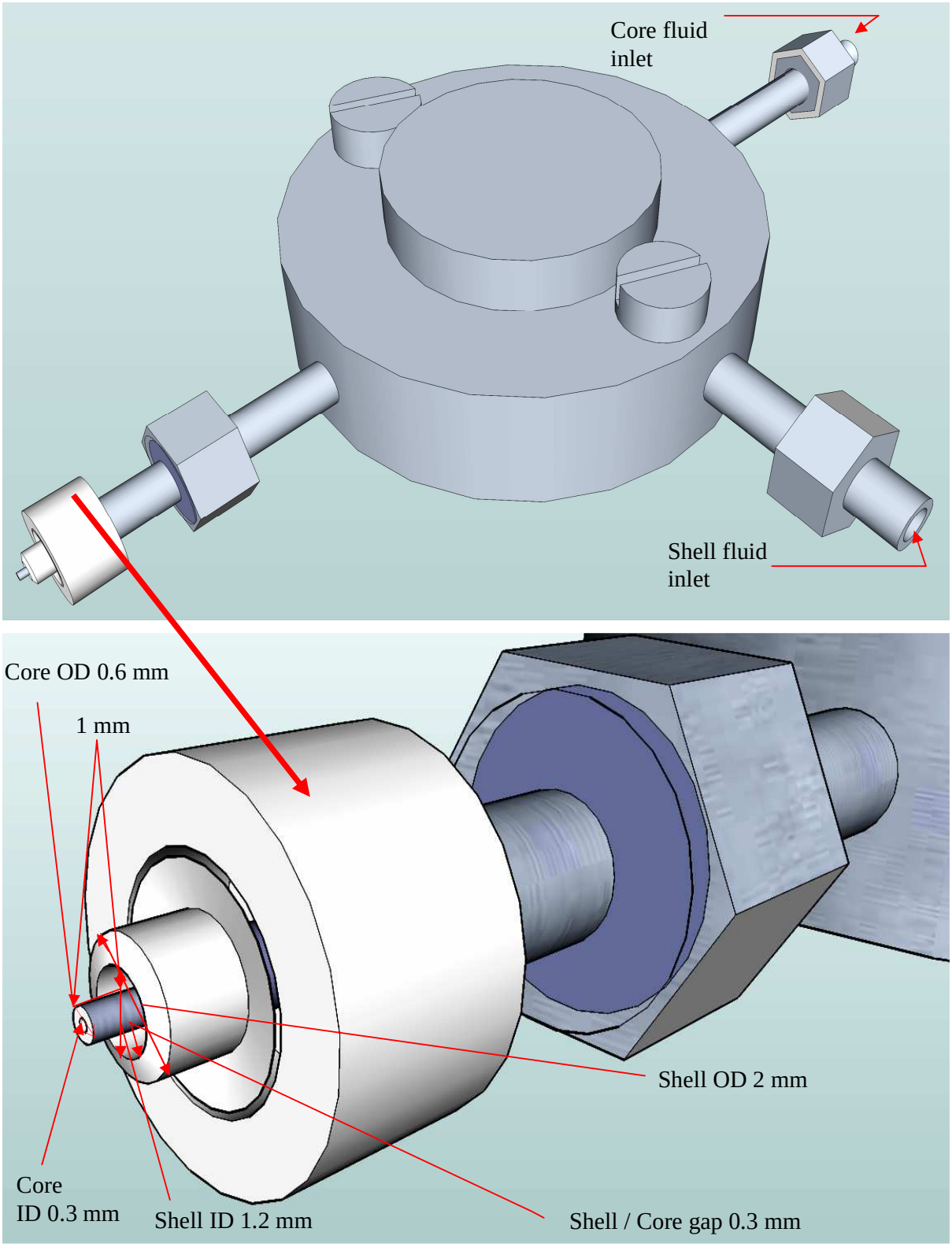

Figure E1: Schematic of coaxial spinneret used in this study.

E.1 Calculating linear velocity

1. Shell linear velocity

The shell capillary inner diameter is 1.2 mm

The shell feed rate is 3 ml/hr

Volume of the shell capillary = (cross-section area) * length

The radius of the shell capillary = 0.6 mm, therefore its cross-sectional area is (πr^2) = 0.36 π

Assuming that 1 ml is equivalent to 1 cm^3, then 3 ml = 3 cm^3 = 3000 mm^3

So the length of tube required to contain 1 hour = 3000/0.36 π = 2655 mm

hence the shell linear velocity is 2655 mm/hr (0.7 mm/s).

2. Core linear velocity

The core capillary inner diameter is 0.3 mm

The core feed rate is 0.5 ml/hr

Volume of the core capillary = (cross-section area) * length

The radius of the core capillary = 0.15 mm, therefore its cross-sectional area is (πr^2) = 0.022 π

Assuming that 1 ml is equivalent to 1 cm^3, then 0.5 ml = 0.5 cm^3 = 500 mm^3

So the length of tube required to contain 1 hour = 500/0.022 π = 7246 mm

hence the core linear velocity is 7246 mm/hr (2 mm/s).